PNE-5011

Plowshare civil, industrial and scientific uses for nuclear explosives

UNITED STATES ARMY CORPS OF ENGINEERS

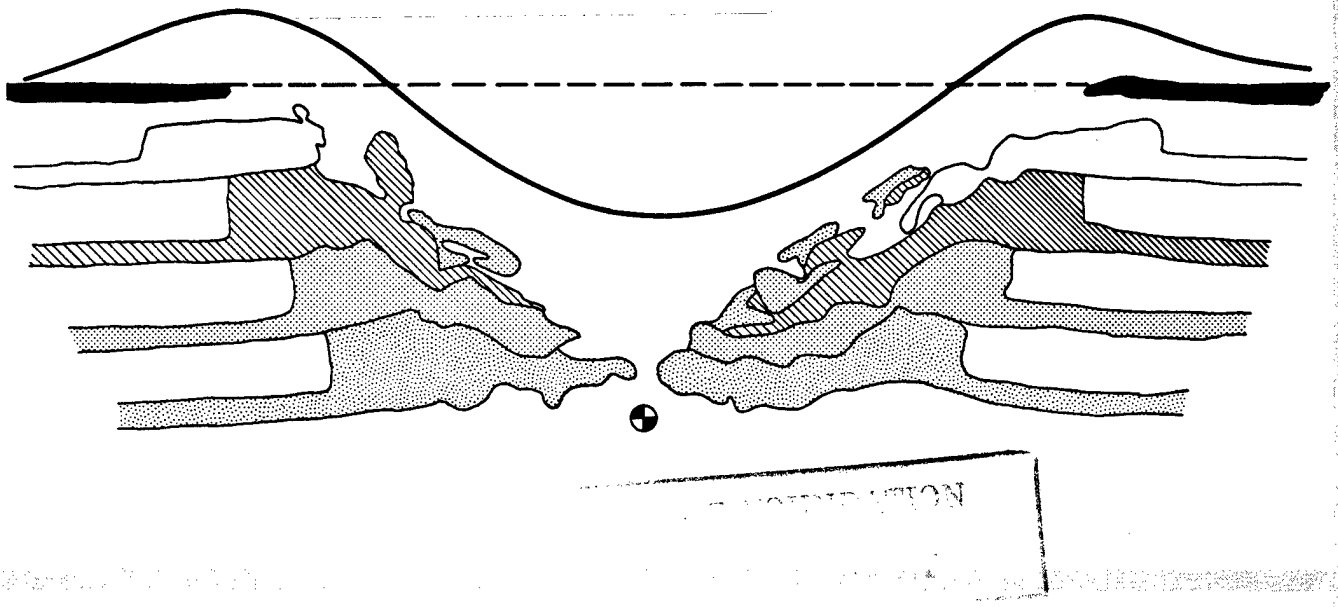

THE FORMATION OF A CRATER AS OBSERVED IN A SERIES OF LABORATORY-SCALE CRATERING EXPERIMENTS

MAJOR ROBERT G. BENING LT. COLONEL MAURICE K. KURTZ, JR.
U.S. Army Engineer Nuclear Cratering Group
Livermore, California

U. S. Army Engineer Nuclear Cratering Group
Livermore, California

ISSUED: OCTOBER 1967

PNE 5011

THE FORMATION OF A CRATER AS OBSERVED IN A SERIES OF LABORATORY-SCALE CRATERING EXPERIMENTS

Major Robert G. Bening
Lt. Colonel Maurice K. Kurtz, Jr.

U. S. Army Engineer
Nuclear Cratering Group
Livermore, California

September 1967

PREFACE

The experimental results and interpretations presented in this report are the outcome of many hours of effort devoted by all those who have participated in the NCG cratering research program. The initial Project Zulu II test program was established by Major B. C. Hughes and continued by Major R. H. Benfer as Deputy for Research. Captain D. D. DeFord, Captain W. G. Christopher, and First Lieutenant K. L. Larner were intimately associated with the supervision of the program. High explosive technical support was supplied by personnel of the University of California Lawrence Radiation Laboratory at the High Explosive Test Facility (Site 300) located near Livermore, California.

The hypothesis of crater formation presented in this report was developed under the guidance of Lieutenant Colonel Walter J. Slazak, Director of NCG during the conduct of this series of experiments.

ABSTRACT

A qualitative description of the formation of a crater is developed on the basis of a series of laboratory-scale cratering experiments. The results of 41 one-pound, single-charge cratering detonations in a concrete sand placed under controlled conditions are summarized. The effect of depth of burst on crater dimensions is illustrated. The crater formed by a one-pound charge buried at a depth of burst of 2 feet is selected for analysis because the ratio of depth of burst to depth of apparent crater is similar to that considered desirable for a prototype nuclear excavation. On the basis of these experiments and a series of gram-size, half-space cratering experiments conducted behind a Plexiglas plate, a description of the formation of a crater is hypothesized. Subsidence or slumping of the cavity walls during the formation of the crater is shown to play an important part in the formational process. The importance of this mechanism to the analysis of crater stability is discussed.

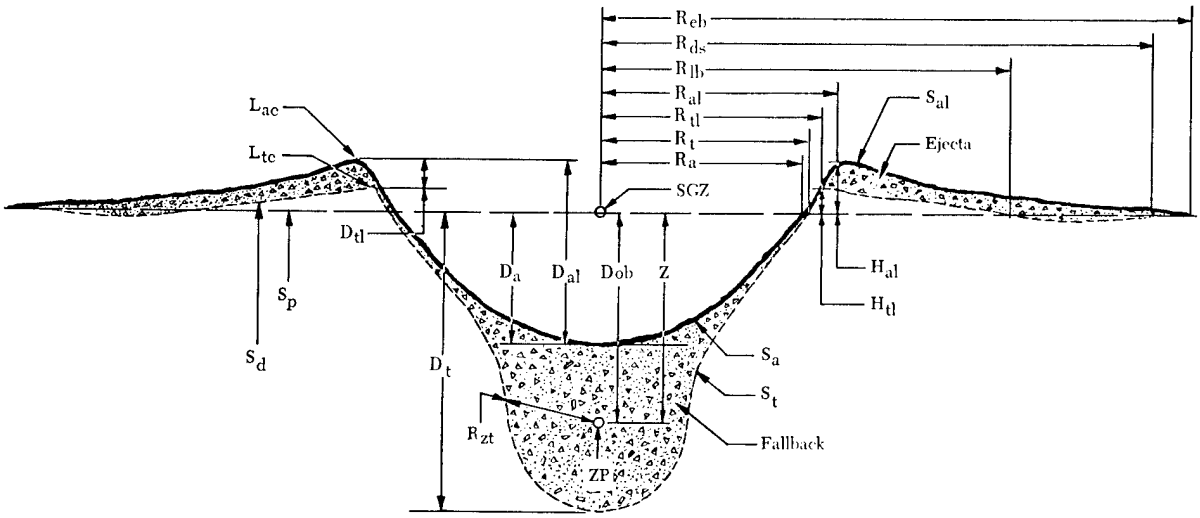

D_a . . . Maximum depth of apparent crater below preshot ground surface measured normal to the preshot ground surface.*

D_{al} . . . Depth of apparent crater below average apparent crater lip crest elevation.

Dob . . Normal depth of burst (measured normal to preshot ground surface).

Dt . . . Maximum depth of true crater below preshot ground surface.

D_{tl} . . . Depth of true crater lip crest below apparent crater lip crest.

Ejecta . Material above and or beyond the true crater and includes: (1) foldback; (2) breccia—ballastic trajectory; (3) dust—aerosol transport: etc.

Fallback. Material fallen inside the true crater and includes: (1) slide blocks; (2) breccia and stratified fallback —ballastic trajectory; (3) dust—aerosol transport: (4) talus; etc.

H_{al} . . . Apparent crater lip crest height above preshot ground surface.

H_{tl} . . . True crater lip crest height above preshot ground surface.

L_{ac} . . . Apparent crater lip crest.

L_{tc} . . . True crater lip crest.

R_a . . . Radius of apparent crater measured on the preshot ground surface.

Note: The radius measurements pertain only to single charge craters and represent average dimensions. If crater shape deviates substantially from circular, the direction of measurement must be specified. An average radius value can also be determined by dividing the plan area by π and taking the square root.

R_{al} . . . Radius of apparent lip crest to center.

R_{ds} . . . Outer radius of displaced surface.

R_{eb} . . . Radius of outer boundary of continuous ejecta.

R_{lb} . . . Outer radius of true lip boundary.

R_t . . . Radius of true crater measured on the preshot ground surface.

R_{tl} . . . Radius of true lip crest to center.

R_{zt} . . . Distance between the zero point and the true crater surface measured in any specified direction. When measured in a direction below the zero point is equivalent to lower cavity radius.

S_a . . . Apparent crater surface, e.g. rock-air or rubble-air interface.

S_{al} . . . Apparent lip surface.

SGZ . . Surface ground zero.

S_d . . . Displaced ground surface.

S_p . . . Preshot ground surface.

S_t . . . . True crater surface, e.g. rock-air or rock rubble interface.

V_a . . . Volume of apparent crater below preshot ground surface.

V_{al} . . . Volume of apparent crater below apparent lip crest.

V_t . . . Volume of true crater below preshot ground surface.

V_{tl} . . . Volume of true crater below true crater lip crest.

Z . . . . Vertical depth of burst (equivalent to Dob when crater is formed on a horizontal surface).

ZP . . . Zero Point—effective center of explosion energy.

Note: The following definitions apply to linear craters only. Linear crater refers to the excavation formed by overlapping crater effects resulting from a row of charges. All above terms applicable to single craters apply also to linear craters with the exception of the radius terms which are replaced by the width terms below.

W_a . . . Width of apparent linear crater measured on the preshot ground surface.

W_{al} . . Width of apparent lip crest measured across linear crater.

W_{ds} . . Width of displaced surface measured across linear crater.

W_{eb} . . Width of outer boundary of continuous ejecta measured across linear crater.

W_{lb} . . Width of true crater outer lip boundary measured across linear crater.

W_t . . . Width of true linear crater measured on the preshot ground surface.

W_{tl} . . . Width of true linear crater lip crest measured across crater.

*All distances, unless specified otherwise, are measured parallel or perpendicular to preshot ground surface.

CONTENTS

CONTENTS (Continued)

CHAPTER 1.
INTRODUCTION

1.1 PURPOSE

This report summarizes the results of a series of 41 one-pound, high-explosive, single-charge cratering experiments, designated Project Zulu II, conducted by the U. S. Army Engineer Nuclear Cratering Group (NCG). The report presents a qualitative description of the formation of a crater as hypothesized from this series of experiments and a series of half-space experiments conducted by Dr. A. S. Vesic, Duke University — formerly of Georgia Institute of Technology (Reference 1). This description provides an insight into the physical characteristics and extent of the various zones surrounding an explosion-produced crater — information essential to the evaluation of the stability of such a crater.

1.2 SCOPE

This report includes (1) a brief description of the Project Zulu II test facility and experimental procedure, (2) a summary of one-pound, single-charge cratering results, (3) a description of the effect of depth of burial on crater dimensions, and (4) a description of the mechanisms of crater formation for a deeply buried cratering detonation of the type contemplated for a prototype nuclear excavation.

1.3 BACKGROUND

Previous large-scale cratering experiments have developed relatively little information on the movement of material beneath the original ground surface during the process of crater formation. No series of large-scale cratering experiments has been conducted in a homogeneous medium at varying depths of burst with the specific purpose of determining the movement and extent of disturbance of subsurface material.

Laboratory-scale cratering experiments provide the opportunity to analyze these phenomena in considerable detail. The results of these experiments provide a rational basis for the design of large-scale experiments to investigate further the hypotheses developed in the laboratory.

As a part of its cratering research program, the NCG is conducting a series of laboratory-scale chemical explosive modeling experiments designated as Project Zulu II. The objectives of Project Zulu II (Reference 2) include (1) investigations of the geometric effects of single and multiple charges in varying terrain and geologic

conditions, (2) studies of the distribution of ejecta from cratering detonations, and (3) investigations of cratering physics.

Project Zulu II is a five-phase program presently in Phase II. The following gives the test series covered in each phase:

Phase I - Single-charge calibration series in a level, homogeneous medium

Phase II - Row-charge calibration series in a level, homogeneous medium

Phase III - Varying charge array series in a homogeneous medium with varying terrain geometries

Phase IV - Varying charge array series in an inhomogeneous medium with both level and varying terrain geometries

Phase V - Design and model test series for specific engineering projects

Phase I of Project Zulu II consisted of the detonation of 14 single, one-pound, high-explosive charges at varying depths of burst. Phase I had the following purposes: (1) to determine the reproducibility of cratering data in the modeling medium, (2) to develop cratering curves (apparent crater radius and depth versus depth of burst) for the laboratory medium, and (3) to accomplish ground surface motion and ejecta studies. Depths of burst ranging from 1.75 to 2.76 feet were investigated in Phase I.

Upon completion of Phase I a series of 12 additional single-charge detonations (designated the "M" series) was completed at depths of burst ranging from 0 to 1.50 feet. On the basis of information gained from these initial series of experiments, a series of special shots (SS) was developed to investigate in considerably more detail the mechanisms of subsidence or slumping. Fifteen detonations were completed using special diagnostic techniques to evaluate subsurface displacements during the process of crater formation.

Since 1962, Dr. A. S. Vesic (Reference 1) has been conducting small-scale cratering experiments under contract to the U. S. Army Engineer Waterways Experiment Station (References 1 and 3). In a recent series of half-space experiments (Reference 1), sponsored by the NCG, the test medium was placed in a box with a transparent (Plexiglas) wall against which a hemispherical charge of 0.837 gram of lead azide was detonated. A number of cratering detonations was completed at varying depths of burst, and the complete history of formation for each cratering event was recorded using high-speed motion picture photography taken through the transparent wall.

This series of half-space experiments and the results of Project Zulu II form the basis for the hypothesis of crater formation presented in Chapter 4.

CHAPTER 2
EXPERIMENTAL PROCEDURE

2.1 DESCRIPTION OF TEST FACILITY

The Zulu II test pit is located at the High Explosive Test Facility (Site 300) of the University of California Lawrence RadiationLaboratory near Livermore, California.

The pit has a width of 30 feet, a length of 60 feet, and an average depth of 5 feet. Figure 2.1 is a sketch showing the layout of the test pit facility. Figure 2.2 shows the facility under construction, and Figure 2.3 shows the test pit prepared for the detonation

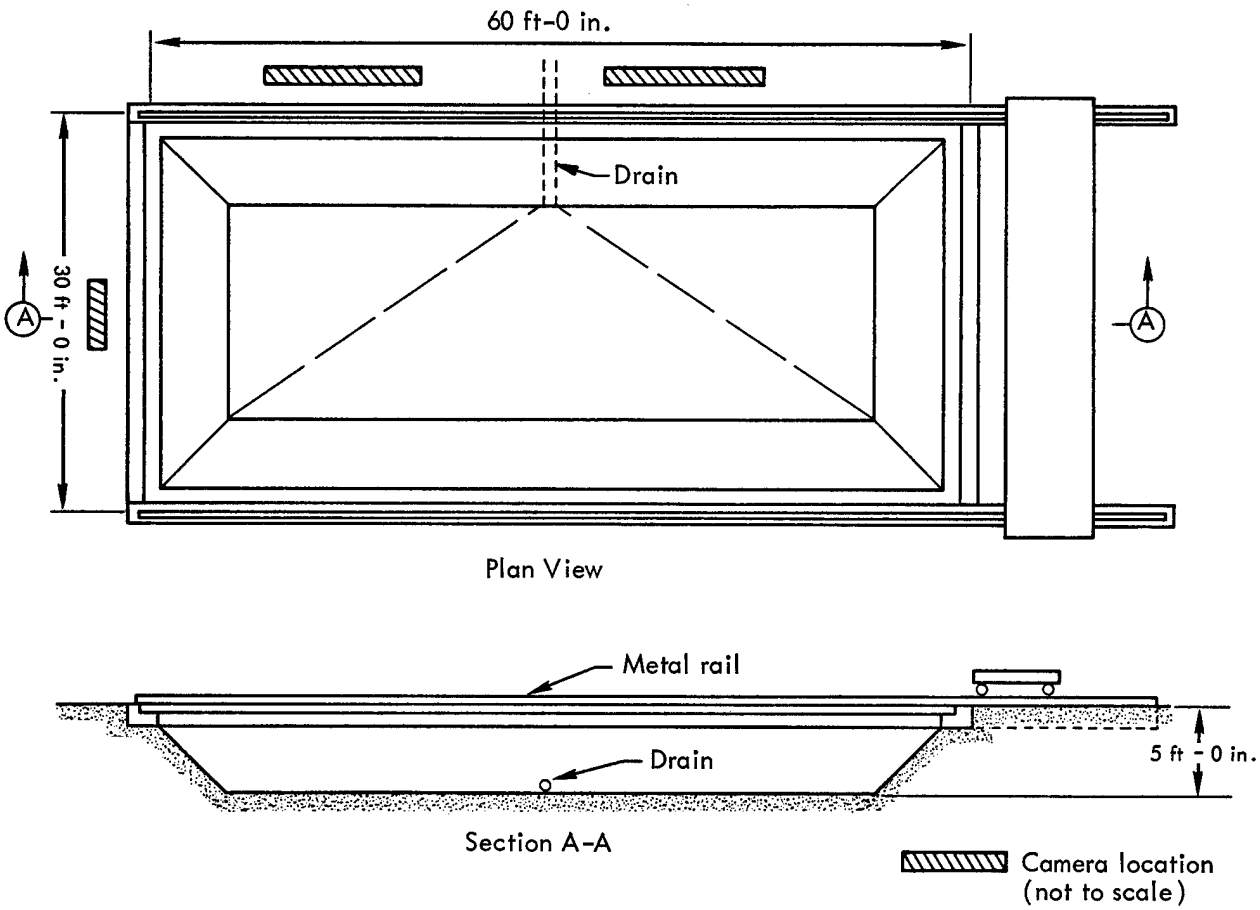

Figure 2.1 Sketch of test pit facility.

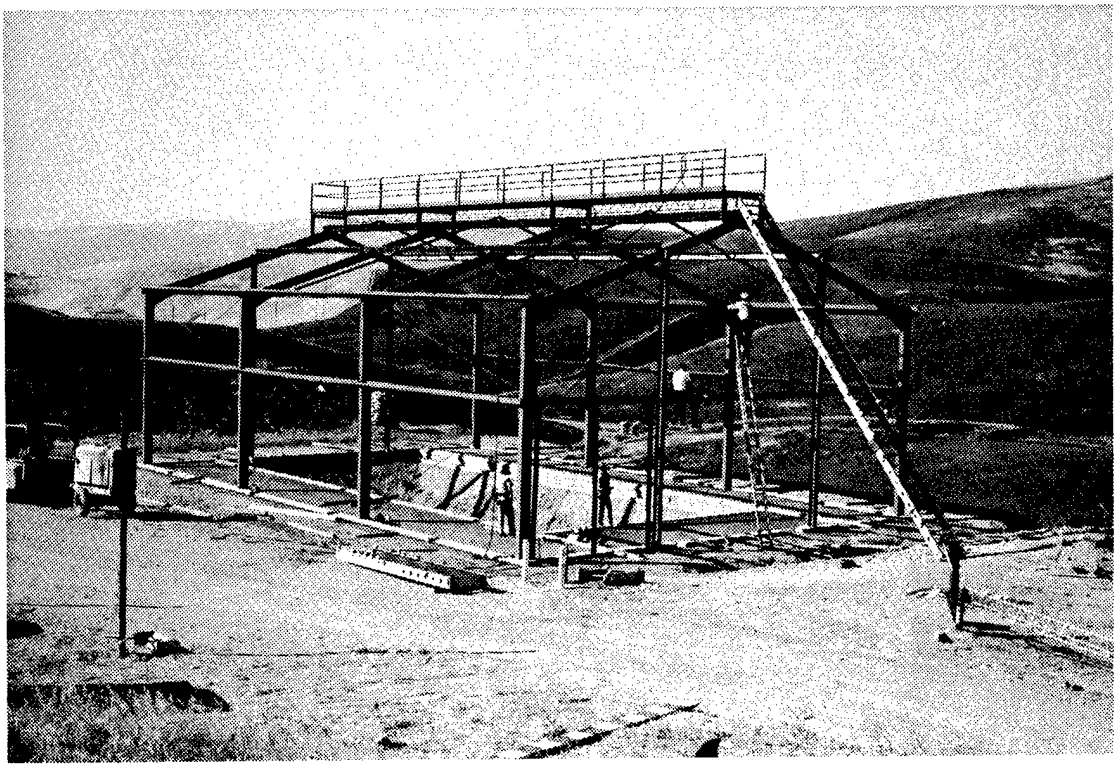

Figure 2.2 Project Zulu II test pit under construction.

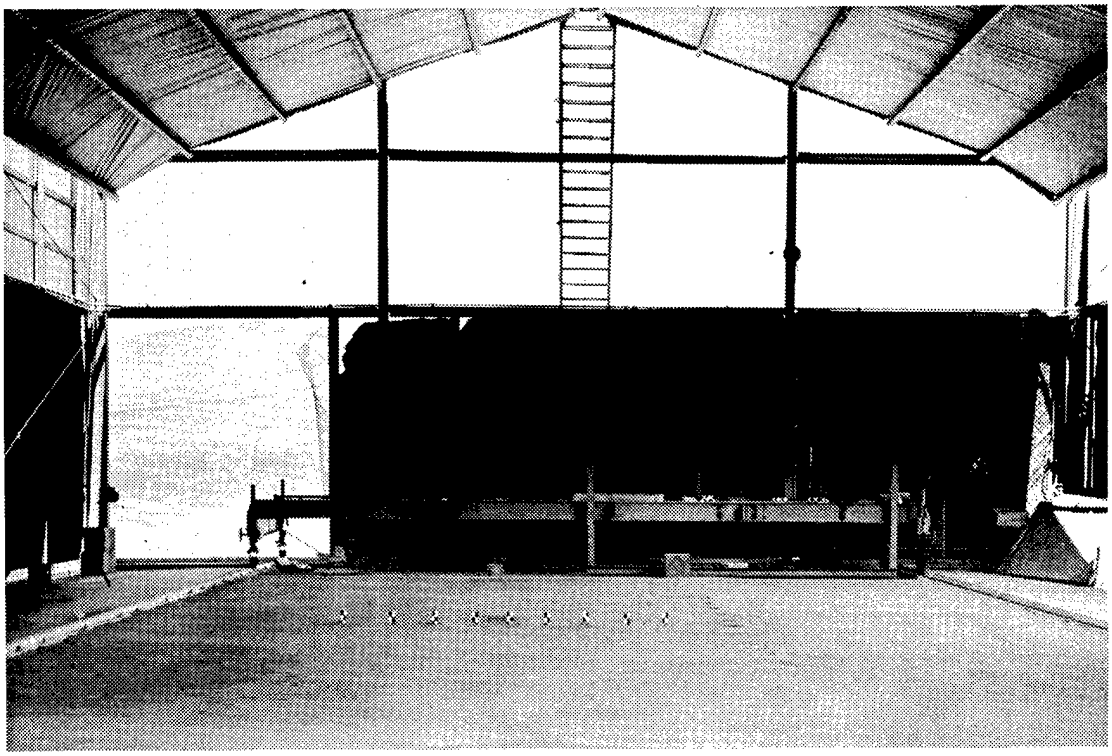

Figure 2.3 Project Zulu II test pit prepared for a detonation.

of a charge. The pit is equipped with a rolling bridge which is used to grade the surface of the pit and as a working platform for postshot surveys. The pit is sheltered by a steel structure with movable canvas roof and side panels, and is equipped with overhead facilities for taking aerial photographs of the craters formed below. These photographs are then used to produce topographic maps for selected experiments.

2.2 DESCRIPTION OF TEST MEDIUM

It was essential that the test medium consist of a material with physical properties which could be easily controlled and reproduced. Project Zulu (Reference 4), a series of one-pound cratering detonations conducted at the Nevada Test Site (NTS), was designed to investigate the suitability of using scalped and remolded desert alluvium as the test medium for Project Zulu II. The poor reproducibility obtained in this preliminary series of tests led to the conclusion that a more easily controlled material should be used. The use of a clean moist sand was recommended.

Extensive laboratory soils tests were performed on two locally available sands by the U. S. Army Engineer Division Laboratory, South Pacific Division, located at Sausalito, California (Reference 5). The tests performed included mechanical analysis, Atterberg Limits, specific gravity, California Bearing Ratio, relative density, compaction, direct shear, and triaxial shear "Q" tests. On the basis of these tests, a concrete sand with the gradation specifications shown in Figure 2.4 was selected as the test medium. The density of the selected gradation showed less sensitivity to variations in moisture content than did that of the other sand tested.

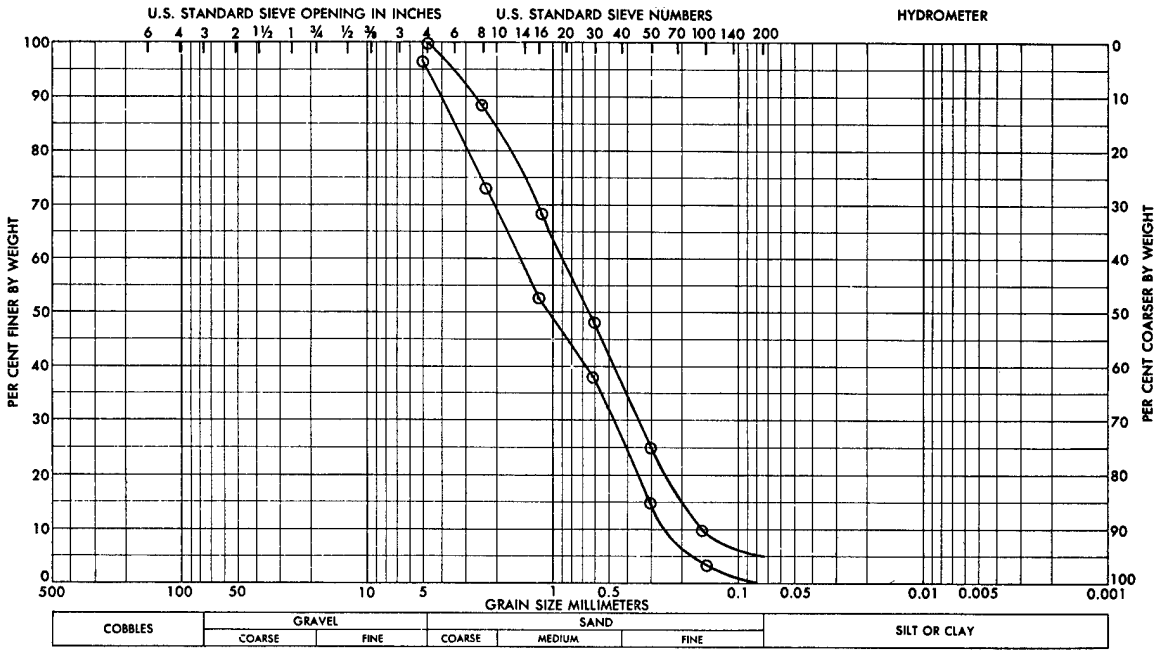

Figure 2.4 Grain size distribution specification.

2.3 QUALITY CONTROL

To insure the reproducibility of test results, it is essential that careful quality control procedures are followed during the placement of the concrete sand in the test pit. Field compaction tests completed by the Corps of Engineers Soils Testing Laboratory showed that 11 passes of a vibratory compactor over a 7-inch lift of loose sand with a moisture content of 6 percent would yield a consistent density. On the basis of these tests, a specification requiring an average moisture content of 6 percent and an average dry density of 112.0 pounds per cubic foot (pcf) was initially adopted. This specification was maintained during the conduct of the first 29 single-charge cratering detonations considered in this report.

In December 1965, it became necessary to revise these specifications due to the increased moisture content of the material as received from the supplier. The revised specification requires a moisture content varying from 6.5 to 8.5 percent and a dry density ranging from 110.0 to 112.0 pcf.

Table 2.1 presents a summary of the average physical properties of the test medium recorded prior to each of the cratering experiments considered in this report.

2.4 DESCRIPTION OF EXPLOSIVE CHARGE

The explosive charge used in all experiments was one pound of C-4 high explosive molded into a thin lucite spherical shell with an SE-1 exploding bridge wire detonator located at its center. All charges were detonated using a capacitor discharge unit (CDU).

After completion of backfill operations, a 4-inch vertical emplacement hole was dug to the prescribed depth of burial. The charge was then emplaced and checked for correct depth of burial. The hole was stemmed to the surface level of the test pit by placing sand over the charge and tamping by hand with a plastic rod.

2.5 TECHNICAL PROGRAMS

A number of technical programs have been developed in conjunction with the Zulu II laboratory-scale cratering experiments. Technical programs implemented during the course of these experiments include the following:

1. Crater measurements
2. Ejecta studies
3. Surface motion studies
4. Colored sand layers

The following paragraphs briefly summarize the scope and objectives of each of these programs. These programs were implemented on a selective basis during the conduct of the series of detonations described in this report.

TABLE 2.1 AVERAGE PHYSICAL PROPERTIES OF TEST MEDIUM

Single Charge No.	Date	Wet Density	Moisture	Dry Density
		lbs/ft^3	%	lbs/ft^3
Zulu II - Single-Charge Cratering Shots				
Original Specifications	2 Aug 65	118.7	6	112.0
1	18 Aug 65	119.4	5.97	112.6
2	18 Aug 65	118.2	6.71	110.9
3	24 Aug 65	118.9	6.01	112.1
4	3 Sep 65	119.6	6.23	112.6
5	3 Sep 65	118.9	5.87	112.2
6	13 Sep 65	120.6	5.99	113.8
7	13 Sep 65	121.3	6.05	114.4
8	24 Sep 65	120.2	5.36	114.1
9	7 Oct 65	117.7	6.01	111.0
10	24 Aug 65	119.2	5.96	112.5
11	20 Sep 65	121.2	5.84	114.4
12-14	Not used	–	–	–
15	20 Sep 65	121.3	6.12	114.3
16	24 Sep 65	112.5	5.96	115.6
17-18	Not used	–	–	–
19	7 Oct 65	117.5	5.94	110.9
"M" Series - Single-Charge Cratering Shots				
M1	20 Oct 65	116.8	5.96	110.2
M2	20 Oct 65	121.6	6.18	114.5
M3	25 Oct 65	116.1	5.76	109.8
M4	25 Oct 65	117.1	6.11	110.4
M5	28 Oct 65	116.6	6.18	110.2
M6	28 Oct 65	116.7	5.53	109.9
M7	3 Nov 65	120.5	6.05	113.6
M8	3 Nov 65	117.1	5.76	110.7
M9	9 Nov 65	117.3	5.51	111.2
M10	9 Nov 65	116.9	5.97	110.6
M11	15 Nov 65	117.5	6.26	110.6
M12	15 Nov 65	116.8	5.61	110.6
Special Shot (SS) - Single-Charge Cratering Shots				
SS5	19 Nov 65	117.3	7.02	109.7
SS7	29 Nov 65	117.5	6.03	110.8
SS8	29 Nov 65	118.4	7.04	110.6
Revised Specifications	8 Dec 65	119.2-121.6	7.5-8.5	110.0-112.0
SS9	17 Dec 65	120.4	7.62	111.9
SS10	17 Dec 65	120.4	7.62	111.9
SS14	18 Feb 66	119.0	7.68	111.6
SS16	21 Feb 66	119.0	7.68	111.6
SS17	29 Mar 66	119.1	6.58	111.8
SS18	29 Mar 66	119.1	6.58	111.8
SS19	14 Apr 66	119.1	7.40	110.9
SS20	14 Apr 66	120.1	7.62	111.8
SS21	4 May 66	119.8	7.60	111.2
SS22	4 May 66	119.8	7.28	111.5
SS24	26 Sep 66	119.4	7.24	111.4
SS26	24 Oct 66	119.6	7.51	111.2

2.5.1 Crater Measurements. This program includes the determination of both the preshot and postshot ground surface profiles. Using conventional survey techniques, profiles are taken along two orthogonal axes through the surface ground zero (SGZ) out to a distance of 12 feet from SGZ. Topographic maps have been prepared for selected experiments using aerial photographs taken from overhead facilities available at the test pit.

In addition to the above-described surface measurements of the apparent crater, the postshot measurements include a "probe profile" taken along the same lines as the surface profiles. The probe, a 1/2-inch square wooden rod, is pushed vertically downward until it is stopped by undisturbed material. Previous experimentation had shown that this probe will penetrate less than 0.03 feet into the preshot surface of the test pit. It was therefore concluded that the "probe profile" obtained by this procedure closely approximates the lower boundary of material significantly disturbed by the detonation.

2.5.2 Ejecta Studies. As a means of determining the origin of material within and surrounding the crater after its formation, ejecta pellets are placed at known locations within the preshot medium. After the detonation, these ejecta pellets are located and their final position recorded.

Numbered bronze spheres are placed within the medium so as to cover the anticipated zone of disturbed material (material ejected from the crater as well as the disturbed material in the zones surrounding the anticipated apparent crater). The spheres are emplaced by pushing them into the surface of each compacted lift of sand during the preparation of the test pit. The preshot location of each sphere is recorded using conventional survey techniques. After the detonation, the location of each sphere ejected from the crater is recorded. The remaining spheres within the disturbed zones adjacent to the apparent crater are located during removal of the sand from the pit, and their final positions are documented.

A detailed analysis of the results of these studies is presented in Reference 6.

2.5.3 Surface Motion Studies. The basic technique used to study ground surface motion consists of:

1. Recording the surface motion using high-speed motion picture photography of the mound growth
2. Analyzing the film to develop the time history of target displacement and to compute the velocity history for each target

Surface motion targets (see Figure 2.3) are placed along an axis through SGZ perpendicular to the line of sight of the camera. The movement of these targets is recorded on high-speed film which is analyzed using a microscope digitizer. These displacement data are analyzed using a digital computer (Reference 7) to develop the velocity history for each target.

2.5.4 Colored Sand Layers. A method of recording movements beneath the surface of the apparent crater was developed using layers of colored sand. Colored sand layers are emplaced within the medium to provide a visual record of displacement. Four layers are emplaced on each side of the proposed shot point. Figure 2.5 shows a typical

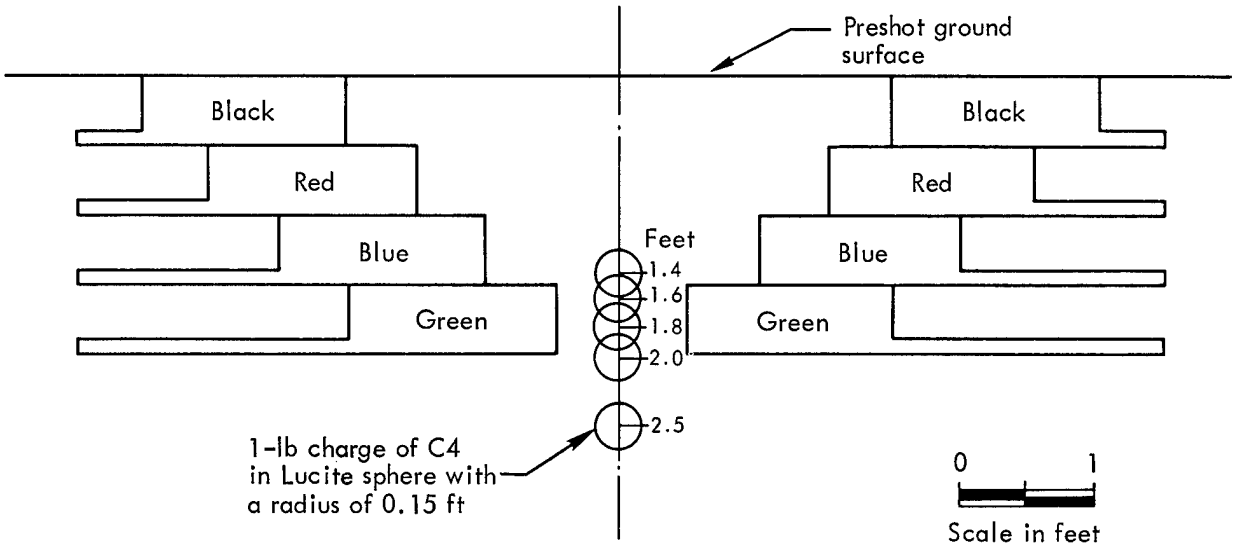

Figure 2.5 Typical layout for colored sand layers.

layout of the sand layers and the relative position of the charge. The bottom layer is 6 inches from the shot point with each succeeding layer recessed an additional 6 inches. The sand is colored by mixing with a water soluble dye at the specified moisture content. The colored sand is then emplaced as part of a regular 7-inch lift and compacted in the normal manner. The colored sand layers are a principal diagnostic technique used in the development of the hypothesis of crater formation presented in Chapter 4.

CHAPTER 3
SUMMARY OF RESULTS

3.1 CRATER MEASUREMENTS

Selected data for those single-charge craters considered in this report are tabulated in Table 3.1. Data are presented for depths of burst ranging from 0 to 2.76 feet. Standard crater nomenclature (see page 4) has been used where possible. It has been necessary to define a number of additional parameters observed in the conduct of these laboratory-scale experiments. Definitions of the parameters tabulated are presented at the end of Table 3.1.

3.2 SURFACE MOTION STUDIES

A detailed analysis of surface motion phenomena is presented in Reference 7. This study concludes that the peak velocity of the SGZ target decays approximately as the cube of the depth of burst (DOB) for Zulu II. An approximate relationship showing the variation in the maximum velocity of the SGZ target with DOB is:

$$V_{max} = \frac{470}{DOB^3}$$

where DOB is in feet and V_{max} is in ft/sec.

The maximum velocity of the SGC target (V_{max}) is presented in Table 3.1. The variation in V_{max} with DOB is clearly illustrated. In all cases where the maximum velocity falls below 40 ft/sec, no crater is formed.

3.3 CRATERING CHARACTERISTICS OF TEST MEDIUM

The results of the crater measurements program presented in paragraph 3.1 form the basis for definition of the cratering characteristics of the test medium. Figure 3.1 is a plot of these data showing the variation of apparent crater radius (R_a) and apparent crater depth (D_a) with DOB. These curves show that the apparent crater of greatest dimension is produced by a DOB of approximately 1.5 feet. At a DOB in excess of 2.11 feet, no apparent crater is formed.

3.4 EFFECT OF VARIATIONS IN DEPTH OF BURST

The previous paragraph describes the variation in apparent crater radius and depth with varying DOB. The extent of disturbed material surrounding the apparent crater also varies with the DOB. The probe profile described in paragraph 2.5.1 defines

TABLE 3.1 SUMMARY OF RESULTS FOR SINGLE-CHARGE CRATERS

All charges were one-pound C-4 spheres center-detonated.

DOB	Shot No.	D_a	R_a	H_{al}	R_{al}	R_{eb}	D_p	R_p	V_{max}
feet		feet	feet	feet	feet	feet	feet	feet	fps
0	M9	0.52	1.48	0.125	2.00	5.00	0.65	4.00	3200
0	M11	0.53	1.34	0.163	1.85	5.00	0.55	3.00	ND
0	M12	0.50	1.44	0.195	2.00	4.75	0.60	2.50	ND
0.50	M6	1.09	2.34	0.240	2.90	8.25	1.20	4.00	ND
0.50	M7	0.98	2.07	0.254	2.83	11.50	1.15	3.62	ND
0.50	M10	1.00	2.28	2.245	2.75	9.45	1.10	3.00	1240
1.00	M2	1.51	2.55	0.220	3.00	9.00	1.65	3.13	ND
1.00	M4	1.55	2.64	0.308	3.43	11.30	1.65	3.50	301
1.00	M5	1.60	2.54	0.283	3.13	9.60	1.75	4.00	ND
1.40	SS18	1.89	2.61	0.290	3.25	14.00	2.10	4.50	174
1.40	SS19	1.92	2.53	0.315	3.40	ND	2.15	5.62	161
1.50	M1	1.74	2.63	0.264	3.25	11.20	1.90	3.13	ND
1.50	M3	1.73	2.46	0.356	3.53	10.80	2.05	4.00	100
1.50	M8	1.76	2.54	0.398	3.20	14.00	2.00	4.13	ND
1.60	SS17	1.97	2.57	0.380	3.38	12.00	2.33	4.63	110
1.60	SS20	1.91	2.55	0.363	3.25	ND	2.41	4.63	90
1.75	15	1.55	2.50	0.394	3.08	9.75	2.40	4.13	80
1.75	8	1.49	2.47	0.301	3.12	9.00	2.50	3.88	70
1.80	SS21	1.51	2.41	0.390	3.00	ND	2.52	4.63	84
1.98	10	1.26	2.27	0.455	3.10	7.50	ND	ND	57
1.99	SS7	0.70	1.99	0.361	2.85	6.63	3.02	3.75	44
2.00	1	1.35	2.25	0.485	3.11	6.75	ND	ND	56
2.00	16	1.17	2.41	0.336	3.00	7.75	2.45	3.50	60
2.00	19	1.08	2.24	0.495	3.00	7.15	2.40	3.87	52
2.00	SS5	1.01	2.18	0.521	2.90	8.75	2.02	4.00	50
2.00	SS10	1.21	2.38	0.326	3.13	8.63	2.40	4.00	53
2.00	SS14	0.85	2.26	0.485	3.25	6.00	2.85	3.88	44
2.00	SS16	1.02	2.44	0.385	3.25	6.00	2.83	4.50	ND
2.01	SS22	0.78	2.07	0.410	3.00	ND	2.72	4.38	56
2.11	SS8	0.78	2.19	0.493	3.05	ND	3.23	3.50	44
2.11	SS9	0.60	1.83	0.426	2.90	7.45	2.56	3.75	45
2.11	SS24	0.40	2.05	0.410	3.00	ND	2.76	4.75	42
2.11	2	0	N/A	0.451	2.98	6.25	ND	ND	40
2.11	9	0	N/A	0.390	2.98	7.25	3.00	3.75	39
2.23	4	0	N/A	0.310	2.98	7.50	2.70	4.13	34
2.24	11	0	N/A	0.311	3.10	6.45	2.60	3.88	40
2.27	3	0	N/A	0.300	3.11	9.50	ND	ND	34
2.50	5	0	N/A	0.361	3.33	7.40	2.90	4.25	28
2.50	6	0	N/A	0.325	3.18	7.00	3.25	4.50	33
2.50	SS26	0	N/A	0.410	3.00	ND	3.45	4.50	36
2.76	7	0	N/A	0.354	3.10	6.75	3.50	4.38	21

ND - No Data collected.

N/A - Not Applicable (no apparent crater formed).

DOB - Depth of burst.

D_a - Apparent crater depth.

R_a - Apparent crater radius.

H_{al} - Height of apparent crater lip.

R_{al} - Radius of apparent lip crest to center.

R_{eb} - Radius of outer boundary of continuous ejecta.

D_p - Maximum depth of probe profile from original ground surface.

R_p - Radius of intersection of probe profile with original ground surface.

V_{max} - Maximum velocity of SGZ target.

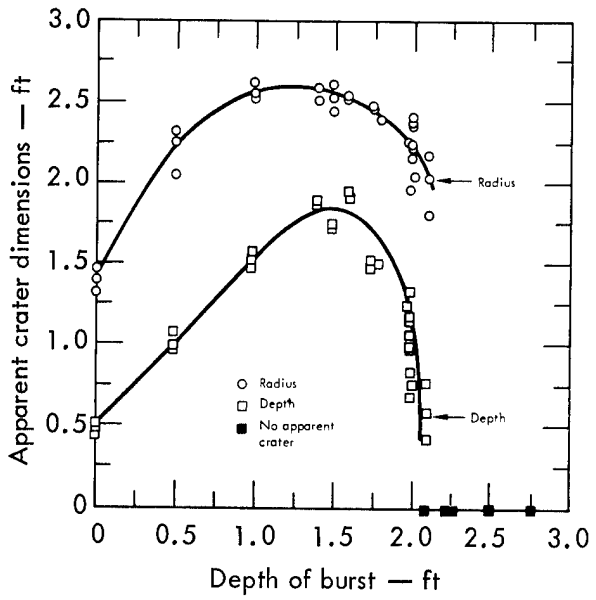

Figure 3.1 Cratering characteristics of Zulu II test medium.

the approximate extent of these disturbed materials. Figures 3.2 through 3.8 show apparent crater cross sections including the probe profile for depths of burst ranging from 0 to 2.76 feet. These figures clearly show the increasing depth of disturbed material with increasing DOB. The depth (D_p) and the radial extent (R_p) of disturbed material are tabulated in Table 3.1.

3.5 RELATIONSHIP TO PROTOTYPE NUCLEAR EXCAVATIONS

The variation in depth of disturbed material relative to the D_a observed in the laboratory-scale cratering experiments is a key factor in relating model results to those anticipated in prototype nuclear excavations. The method developed for relating model to prototype for the purpose of this study is based upon geometric similarity. The ratio of the D_a to the DOB has been selected as a suitable parameter defining this similarity.

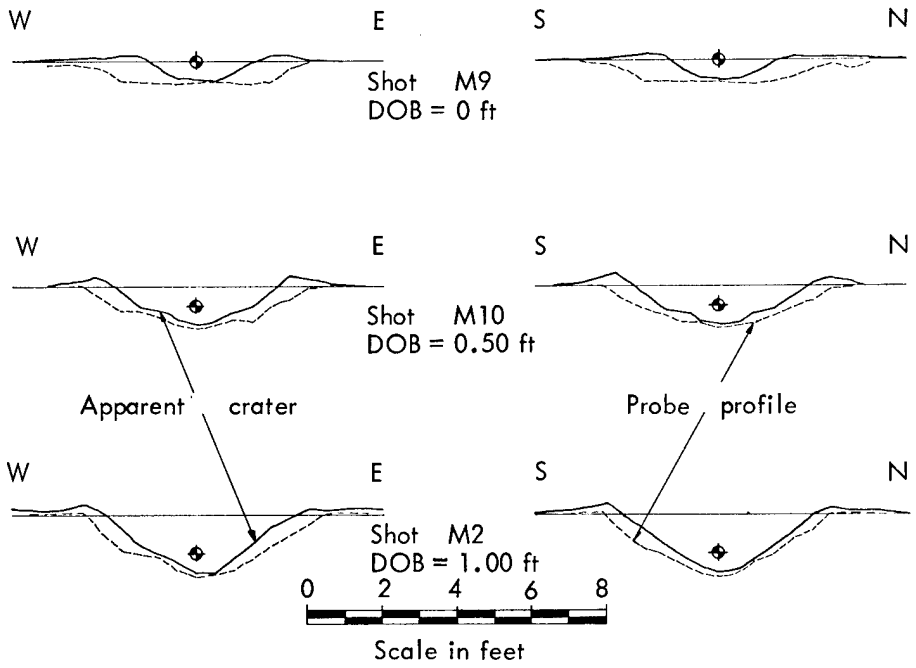

Figure 3.2 Apparent crater cross sections, DOB = 0, 0.50, and 1.00 feet.

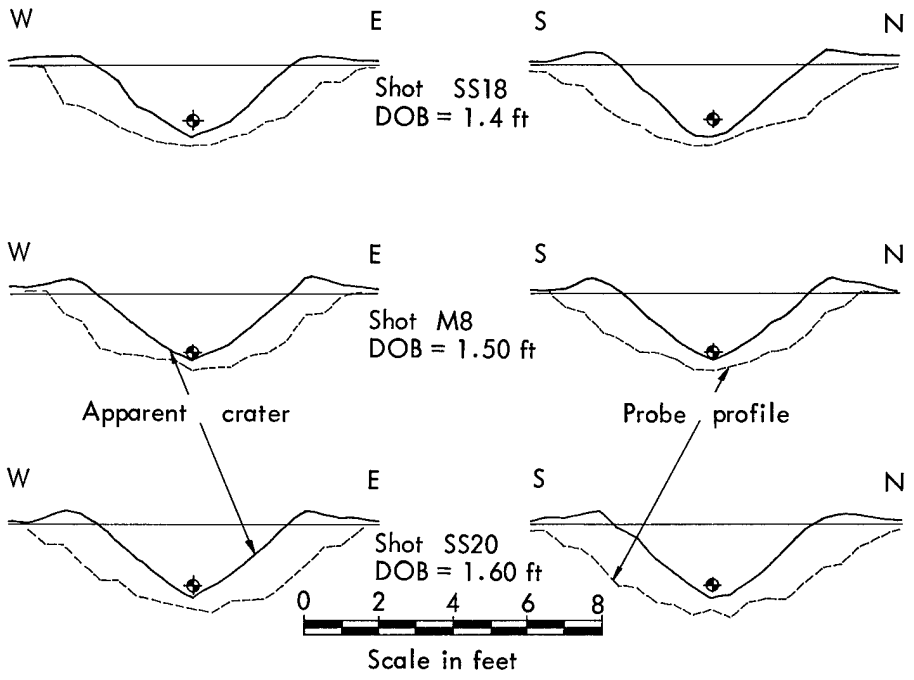

Figure 3.3 Apparent crater cross sections, DOB = 1.40, 1.50, and 1.60 feet.

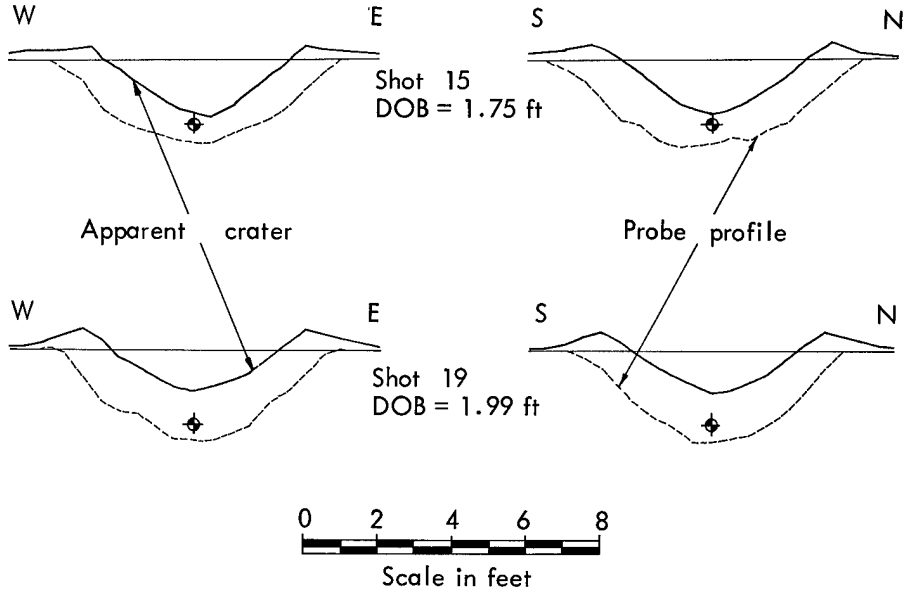

Figure 3.4 Apparent crater cross sections, DOB = 1.75 and 1.99 feet.

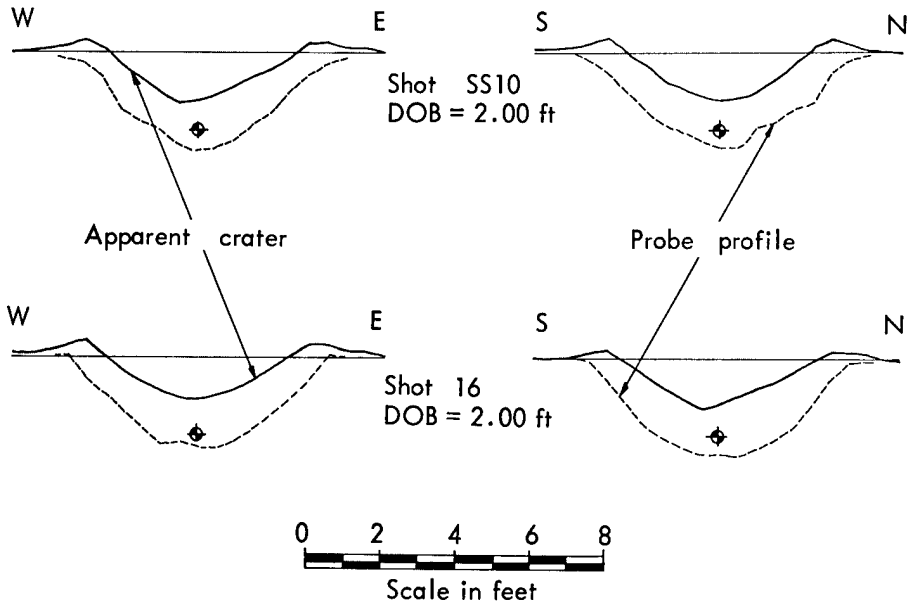

Figure 3.5 Apparent crater cross sections, DOB = 2.00 feet.

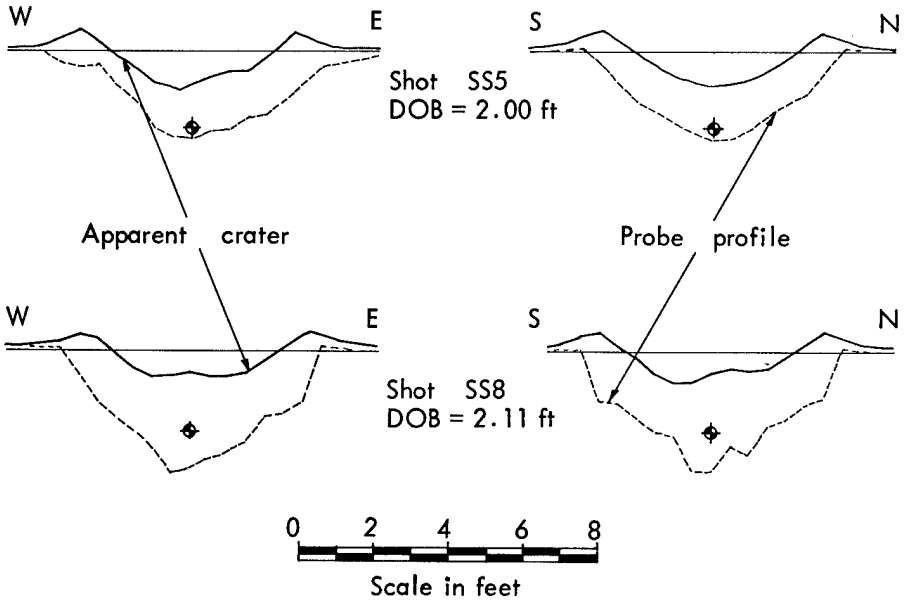

Figure 3.6 Apparent crater cross sections, DOB = 2.00 and 2.11 feet.

The Danny Boy Event (Reference 8) was a 0.42-kt nuclear cratering detonation in basalt. The Sedan Event (Reference 9) was a 100-kt nuclear cratering detonation in desert alluvium. Both events were detonated at NTS and represent the most pertinent nuclear cratering experience to date. In both of these craters a large amount of highly

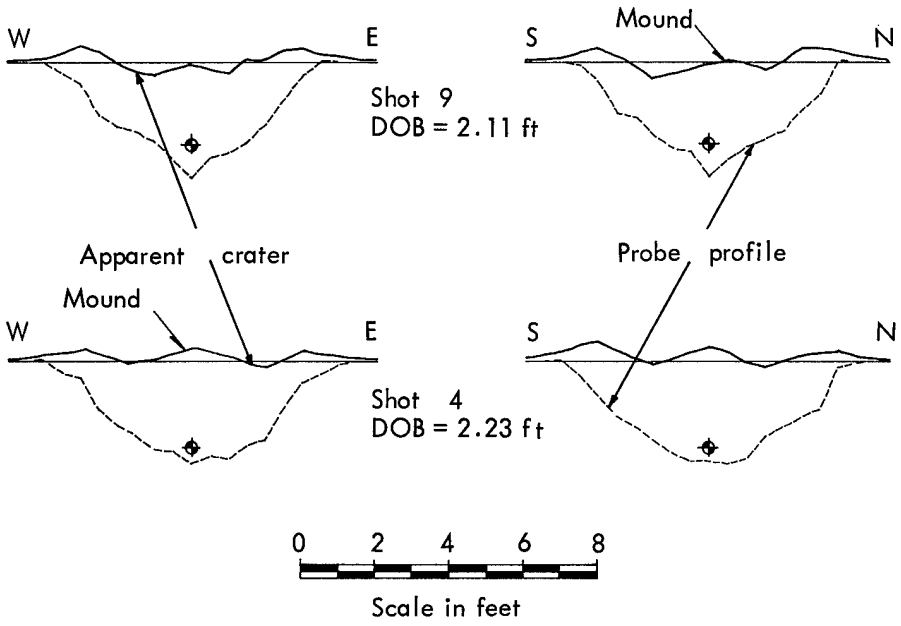

Figure 3.7 Apparent crater cross sections, DOB = 2.11 and 2.23 feet.

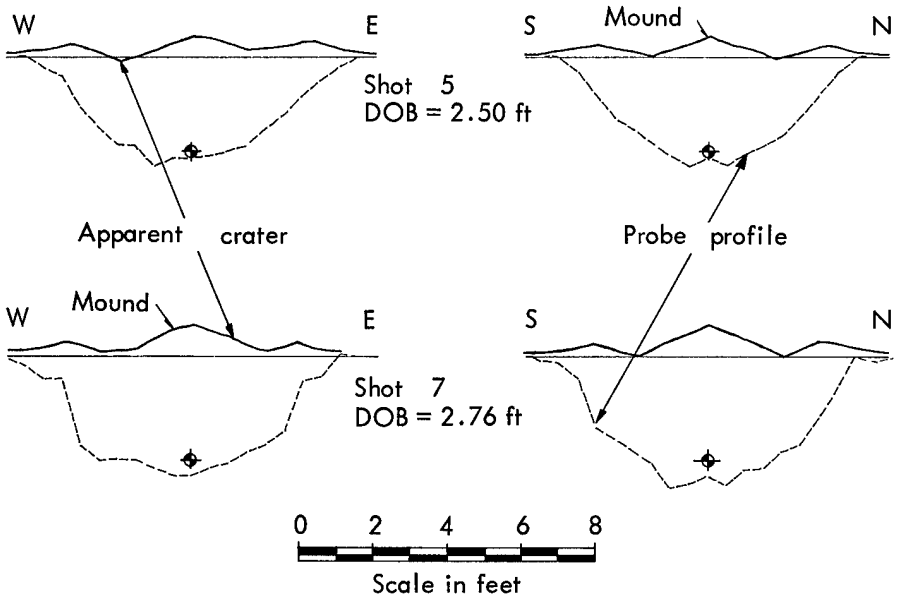

Figure 3.8 Apparent crater cross sections, DOB = 2.50 and 2.76 feet.

disturbed material is present in the bottom of the apparent crater. These events were detonated at a DOB sufficiently deep to insure the entrapment of a major portion of the radioactivity beneath the disturbed materials in the crater bottom.

The Danny Boy crater was produced by a 0.42-kt device buried at a depth of 110 feet. The resulting crater has an R_a of 107 feet and a D_a of 62 feet. The resulting ratio of D_a/DOB is 0.56.

The Sedan crater was produced by a 100-kt device buried at a depth of 635 feet. The resulting crater has an R_a of 600 feet and a D_a of 320 feet. The resulting ratio of D_a/DOB is 0.50.

Table 3.2 is a summary of the results of a similar evaluation using the crater dimensions of the one-pound, laboratory-scale cratering experiments for depths of burst ranging from 1.75 to 2.11 feet. This table shows that for a 2.0-foot DOB the average value of D_a/DOB is 0.52. This value is comparable to the observed values for both Sedan and Danny Boy. On the basis of the geometric similarity between the 2.0-foot DOB and these nuclear detonations, the 2.0-foot DOB has been selected for further detailed study.

TABLE 3.2 COMPARISON OF D_a/DOB FOR SINGLE-CHARGE CRATERS

Shot No.	DOB (ft)	D_a (ft)	D_a/DOB	Average D_a/DOB
		One-Pound High Explosive Single Craters		
8	1.75	1.55	0.89	0.87
15	1.75	1.49	0.85	
SS21	1.80	1.51	0.84	0.84
10	1.98	1.26	0.64	0.52
SS7	1.99	0.70	0.35	
1	2.00	1.35	0.67	
16	2.00	1.17	0.58	
19	2.00	1.08	0.54	
SS5	2.00	1.01	0.51	
SS10	2.00	1.21	0.60	
SS14	2.00	0.85	0.42	
SS16	2.00	1.02	0.51	
SS22	2.00	0.78	0.39	
SS8	2.11	0.78	0.37	0.17
SS9	2.11	0.60	0.28	
SS24	2.11	0.40	0.19	
2	2.11	0.00	0	
9	2.11	0.00	0	
		Nuclear Craters		
Sedan (100 kt)	635	320	0.50	0.50
Danny Boy (0.42 kt)	110	62	0.56	0.56

CHAPTER 4
FORMATION OF A CRATER

4.1 GENERAL BACKGROUND

Several mechanisms of crater formation are defined in References 10 and 11. These mechanisms are (1) crushing, compaction, and plastic deformation of the medium surrounding the explosive source, (2) spall, (3) gas acceleration, and (4) subsidence or slumping. All of these phenomena have been observed to some degree in the series of laboratory-scale experiments described in this report. Postshot excavation in the vicinity of the shot point has shown evidences of the crushing and compaction phenomena. The mechanisms of spall and gas acceleration are clearly evident in the results of the ground surface motion analysis presented in Reference 7. The mechanism of subsidence or slumping of the cavity walls has been observed through the use of colored sand layers emplaced within the test medium (Reference 12).

In general, the mechanism of subsidence or slumping has not been recognized as a significant factor in the formation of an explosion crater except in the case of very deep depths of burial (Reference 10). The results of the one-pound series of experiments indicate subsidence or slumping does play a major role in the formation of an explosion crater when the explosive charge is buried at or slightly below optimum depth of burial, as would be the case in a prototype nuclear excavation project (paragraph 3.5).

Russian investigators (References 13 and 14) have also observed this mechanism to be significant in the formation of a crater. Reference 14 states:

> "The Institute of the Physics of the Earth has recently conducted a series of experiments which show that landslides play a significant role in the formation of the visible ejection crater. Even a crater developed as a result of a blast near the horizontal free surface has quite steep edges at the outset. In some cases, the edges of such a crater are practically vertical, and the shape of the crater approaches that of a cylinder with a truncated bottom. Only the subsequent sliding of steep edges lends its characteristic cup-shaped contour to the ejection crater."

The first series of experiments conducted by Dr. Vesic (Reference 3) also indicates that the mechanism of subsidence or failure of the cavity walls is a significant factor. Figure 4.1 shows the cross section of a crater formed by the detonation of a spherical charge of 1.677 grams of lead azide at a DOB of 2.6 inches in a very dense sand. The sand was placed in colored layers which clearly show the residual displacements beneath the apparent crater.

In a more recent series of experiments (Reference 1), a half-space technique has been developed which permits the recording of the entire process of crater formation using

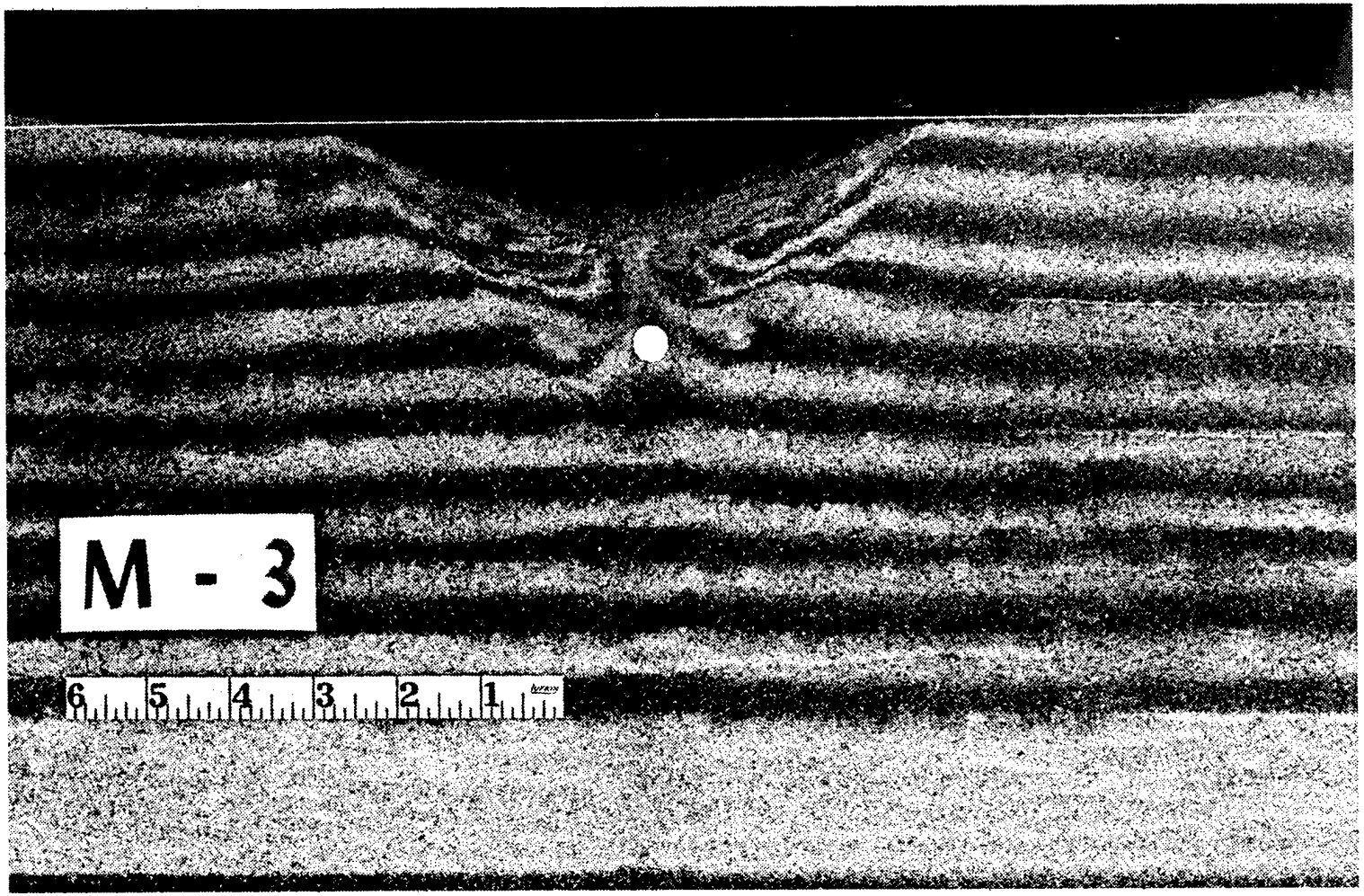

Figure 4.1 Residual displacements around crater in dense sand.

high-speed motion picture photography. This high-speed photography clearly shows that for a cratering detonation at or slightly below optimum depth of burial, the mechanism of subsidence or slumping plays a significant role in the process of crater formation. Figure 4.2 shows the final configuration resulting from the detonation of a hemispherical charge of 0.837 gram of lead azide in dry sand at a depth of burial of 4 inches.

The following paragraphs present a hypothesis of crater formation which shows qualitatively the relative significance of the mechanism of subsidence or slumping in the overall process of crater formation.

4.2 A HYPOTHESIS OF CRATER FORMATION

The series of experiments described in Chapters 2 and 3 and the half-space series of experiments described in the previous paragraph provide the basis for a hypothesis of crater formation. The following paragraphs and associated series of figures describe in detail the formation of a crater as hypothesized from these experiments. The one-pound series of experiments has been used as the model for this description. The high-speed motion picture photography of the half-space experiments has been related to the surface motion photography of the one-pound series experiments to develop a detailed description of the intermediate stages of crater formation. The times shown on the figures are based upon the surface motion photography from the one-pound series of experiments.

4.2.1 Preshot Configuration (Figure 4.3). This figure portrays a cross section through the shot point and shows the colored sand layers as emplaced during the preparation of the test pit. A one-pound charge of composition C-4 is shown buried 2 feet below the level ground surface.

4.2.2 Spherical Cavity Expansion (Figure 4.4). This figure shows the deformation of the medium after 4 msec. The cavity has expanded, and the material is deformed with spherical symmetry.

The shock wave released by the explosion initially produces compression in the medium. The amplitude of this compression decreases away from the shot point. The reflection of the shock wave from the free surface results in a tensile or rarefaction wave which causes cracking of the medium roughly parallel to the free surface. This phenomenon, known as spalling, imparts an upward velocity to the material at and near the surface.

4.2.3 Surface Spall and Upward Cavity Expansion (Figure 4.5). This figure shows appreciable deformation of the ground surface due to the upward expansion of the gas cavity toward the nearest free surface and due to the spalling of the near surface particles.

4.2.4 Gas Acceleration Begins; Subsurface Deformation Continues (Figure 4.6). This figure shows the development of the mound and the cavity which is being formed by the adiabatic expansion of the gases generated by the explosion. The mound is being

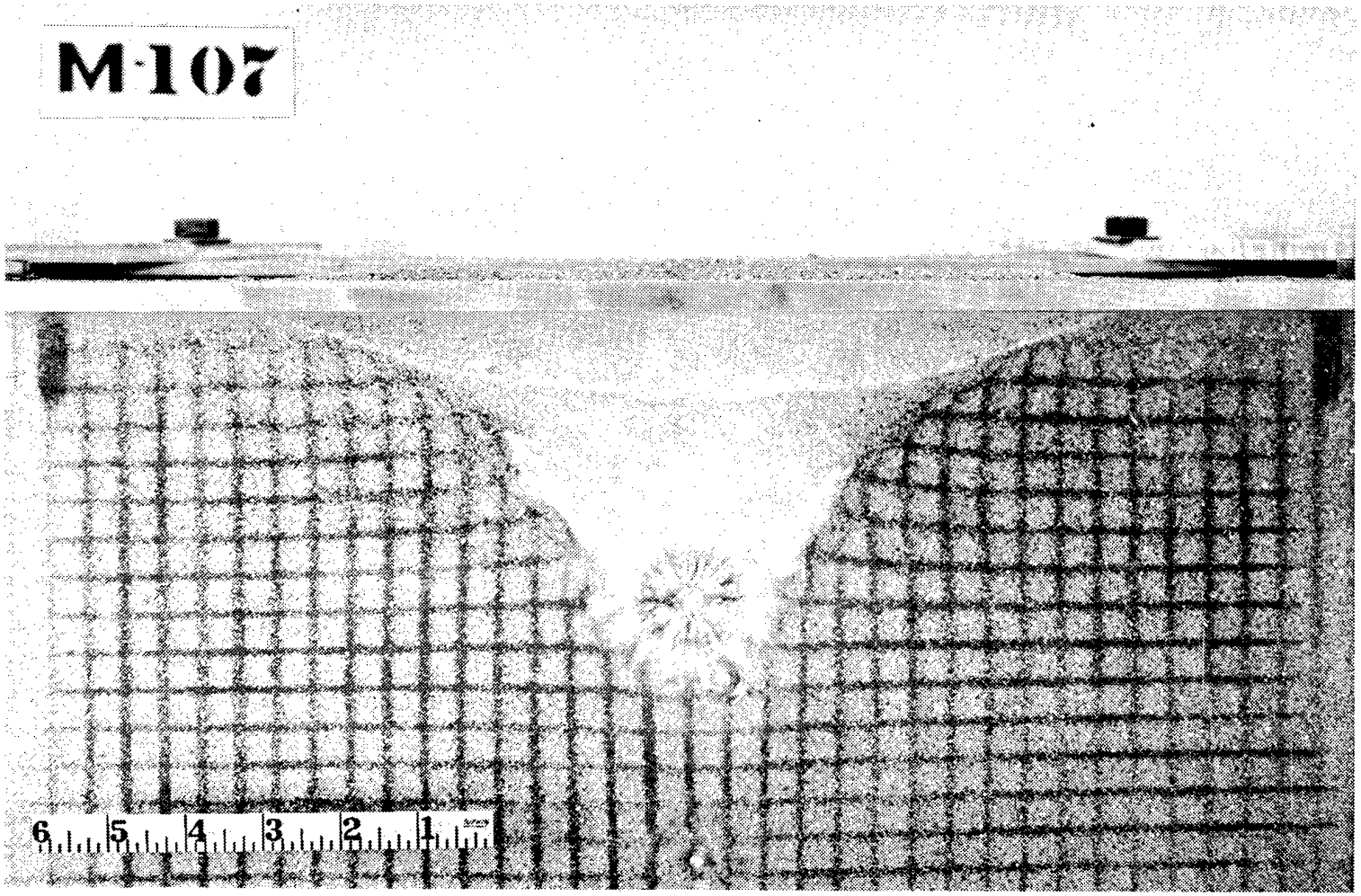

Figure 4.2 Final configuration of half-space crater in dry sand.

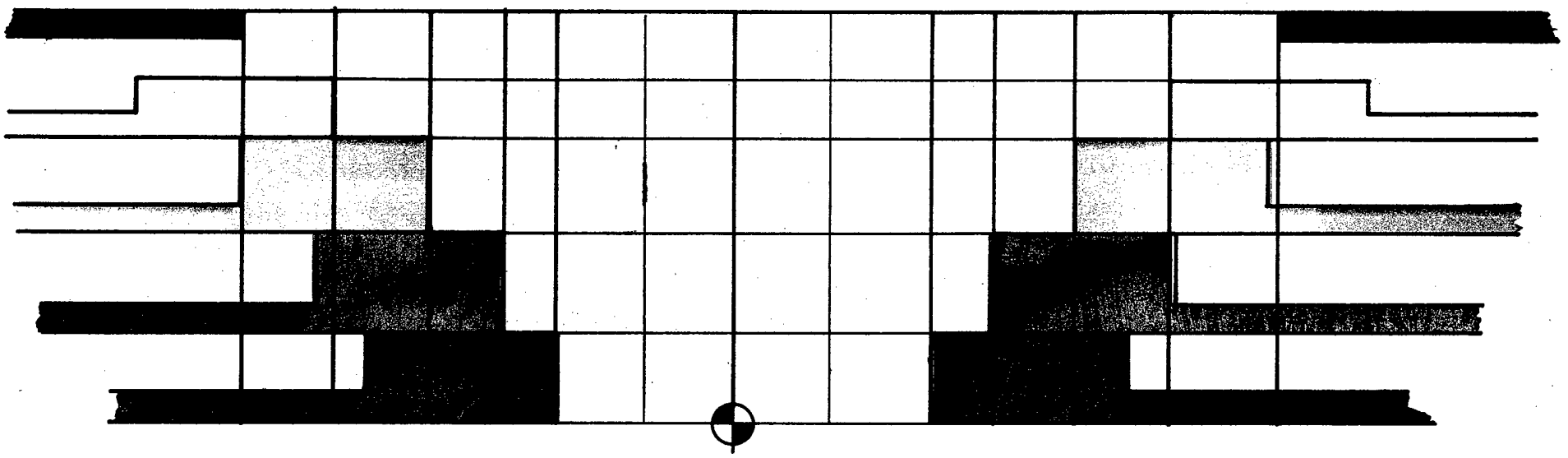

Figure 4.3 Preshot configuration.

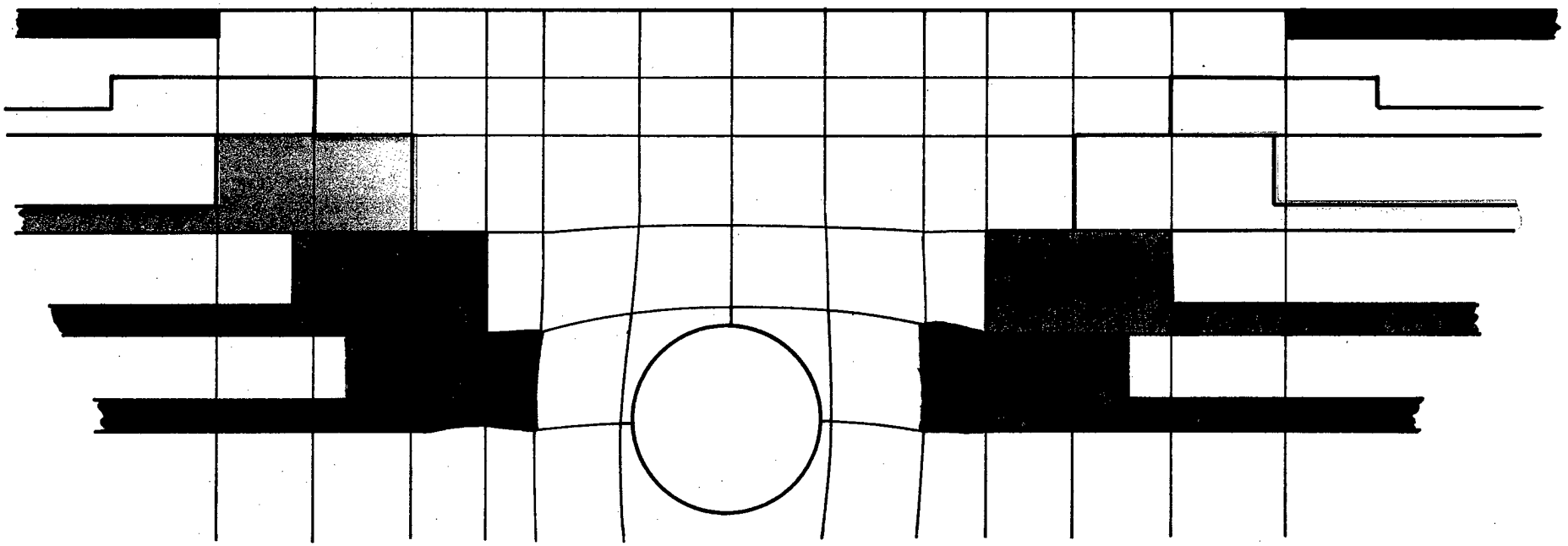

Figure 4.4 Spherical cavity expansion (0 to 4 msec).

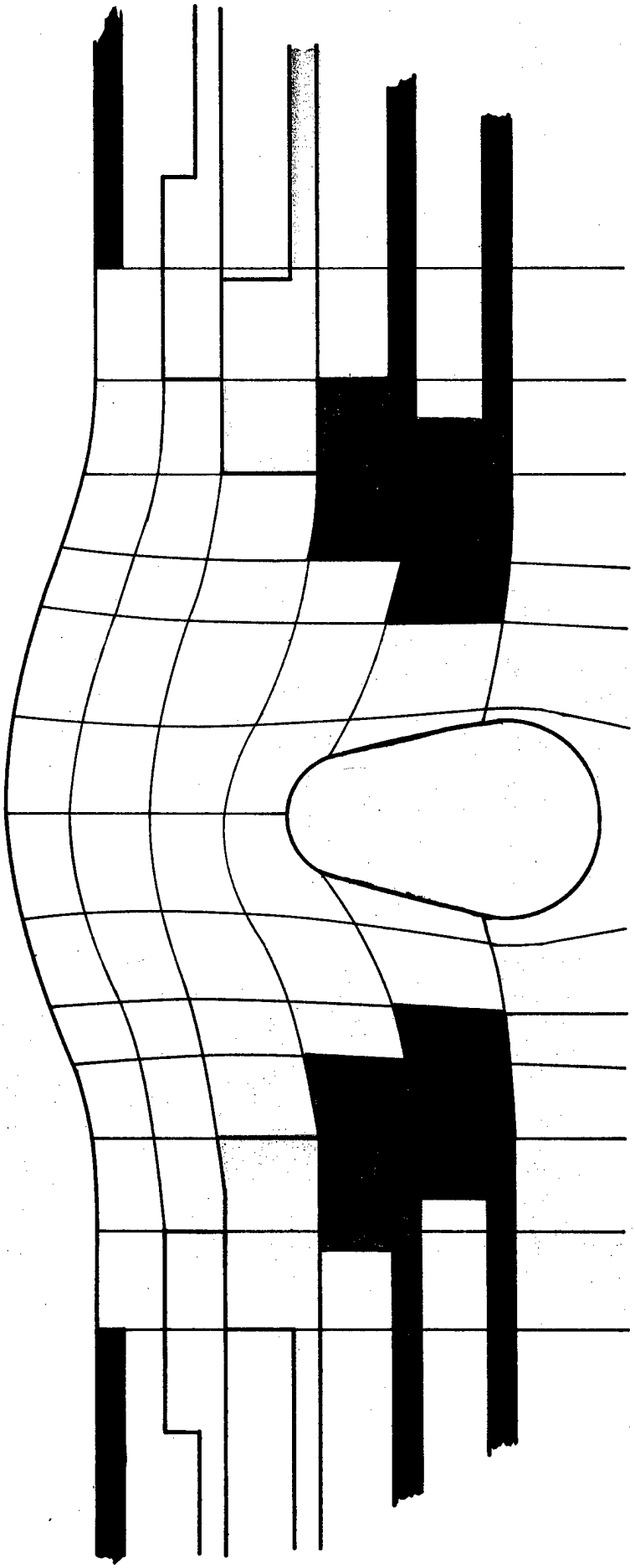

Figure 4.5 Surface spall and upward cavity expansion (10 to 20 msec).

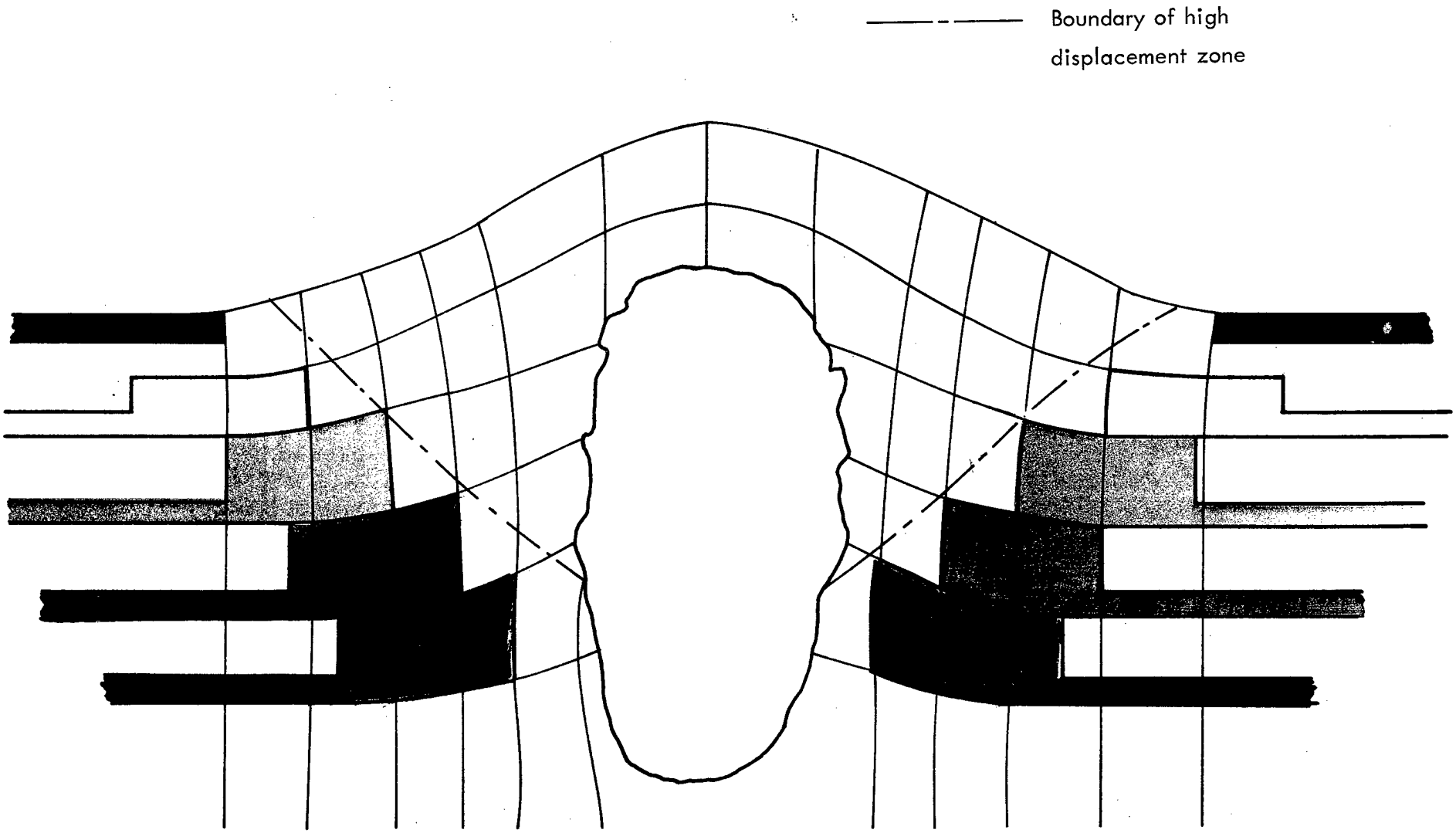

Figure 4.6 Gas acceleration begins; subsurface deformation continues (25 to 35 msec).

accelerated by the expanding gases, and the sand layers are beginning to show uplift. The dash-dot line, bounding the inverted cone region, is estimated to be the boundary between material which is highly deformed and displaced and less severely displaced material. The velocities decrease away from the vertical axis of symmetry and appear to decrease with depth except in the region directly above the gas cavity.

4.2.5 Gas Acceleration and Subsurface Deformation Continue (Figure 4.7). This figure shows the upward and outward expansion of the cavity. The motion is predominantly upward; however, the gas now expands outward into the relatively loose material in the zone of high displacement. The expansion of the high-pressure gas cavity is accompanied by severe turbulence and erosion of the sand along the cavity boundary. The material directly above the cavity is in compression as evidenced by the relatively long period of acceleration of the ground surface particles indicating the effect of gas acceleration rather than spall. The severely deformed region surrounding the cavity has experienced a combination of both shearing and tensile stresses. Beyond the severely deformed region, the medium has been uplifted and displaced away from the shot point.

4.2.6 Mound Growth Continues at Peak Velocity; Rebound Begins at Mid-Depth (Figure 4.8). The cavity pressures have decreased to the point where the mound is no longer accelerating. The lateral pressures have subsided allowing the material at intermediate depth (0.50 to 2.00 feet) to relax inward. In this figure, small portions of several of the sand layers are within the zone of high velocity or significant displacement. The cavity region contains individual particles and clods of sand eroded from the cavity walls. The motion of the sand in this region is not likely to be uniform and would have velocities generally lower than those of the material in the zone directly above the cavity. The bottom spherical portion of the cavity is beginning to fill with the bulked, baked sand from near the shot point.

4.2.7 Shearing Along Boundary of Severe Deformation (Figure 4.9). This figure shows the uplifted material in the walls of the cavity as it reaches the point of maximum uplift and begins to settle. Portions of the sand layers within the high velocity zone continue to move upward (and slightly outward). Because of their large displacements and higher velocities, these fragments begin to lose their shape.

4.2.8 Beginning of Slump Along Free Surface Slopes (Figure 4.10). This figure shows that the sand layers have settled slightly although they are still bulked and uplifted. A free surface with a relatively large slope angle (about 50 degrees) has been formed at the cavity boundary. Considering that the sand is bulked and in motion, failure of the cavity walls is imminent. The corners which have sheared off have become shapeless masses which are still moving upward with the gas and highly displaced material because of their higher velocities.

4.2.9 Continuing Slump Along Free Surface Slopes: Material Fallback Begins (Figure 4.11). This figure shows the slumping of the cavity walls as the pressure of the

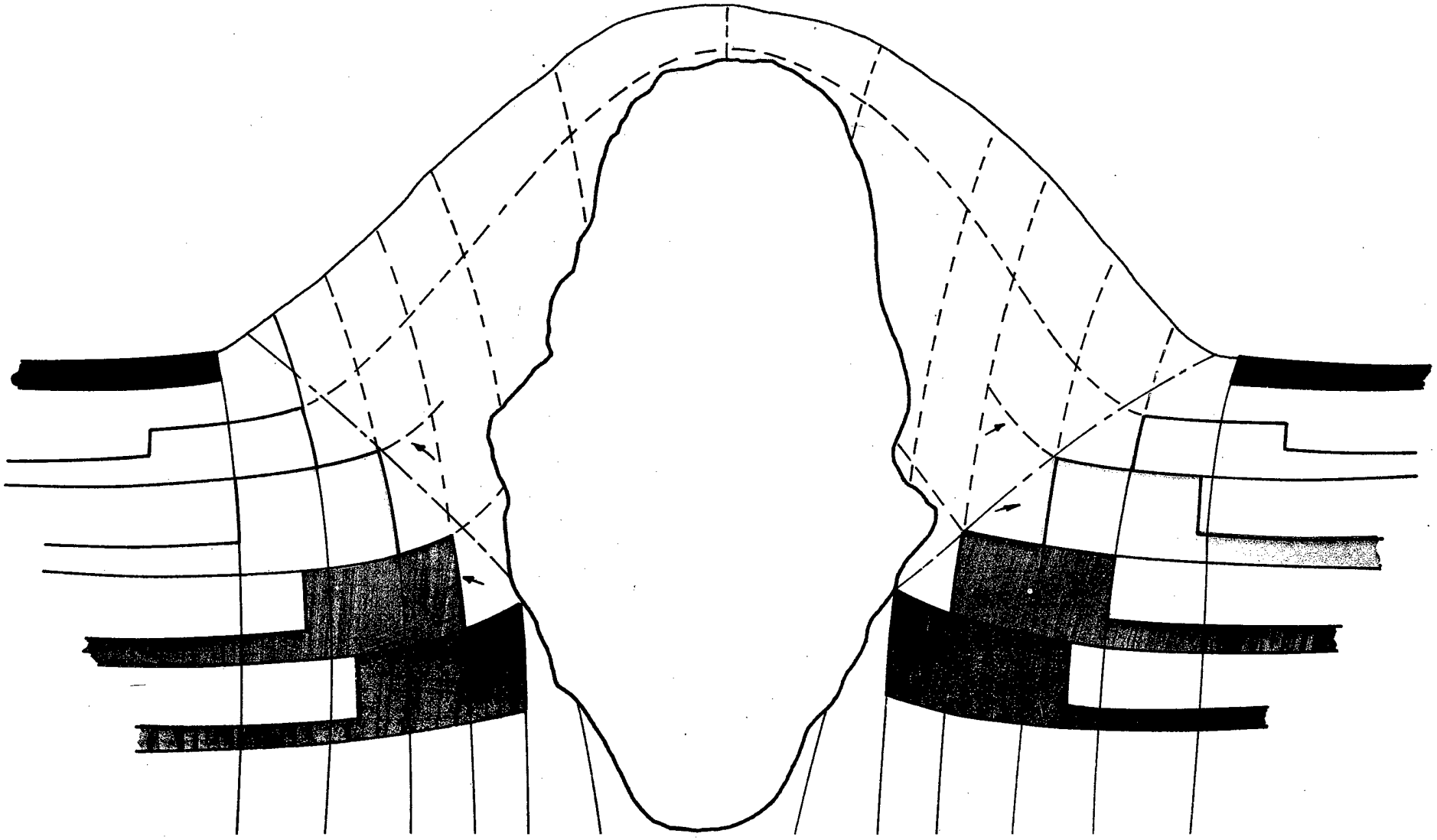

Figure 4.7 Gas acceleration and subsurface deformation continue (40 to 50 msec).

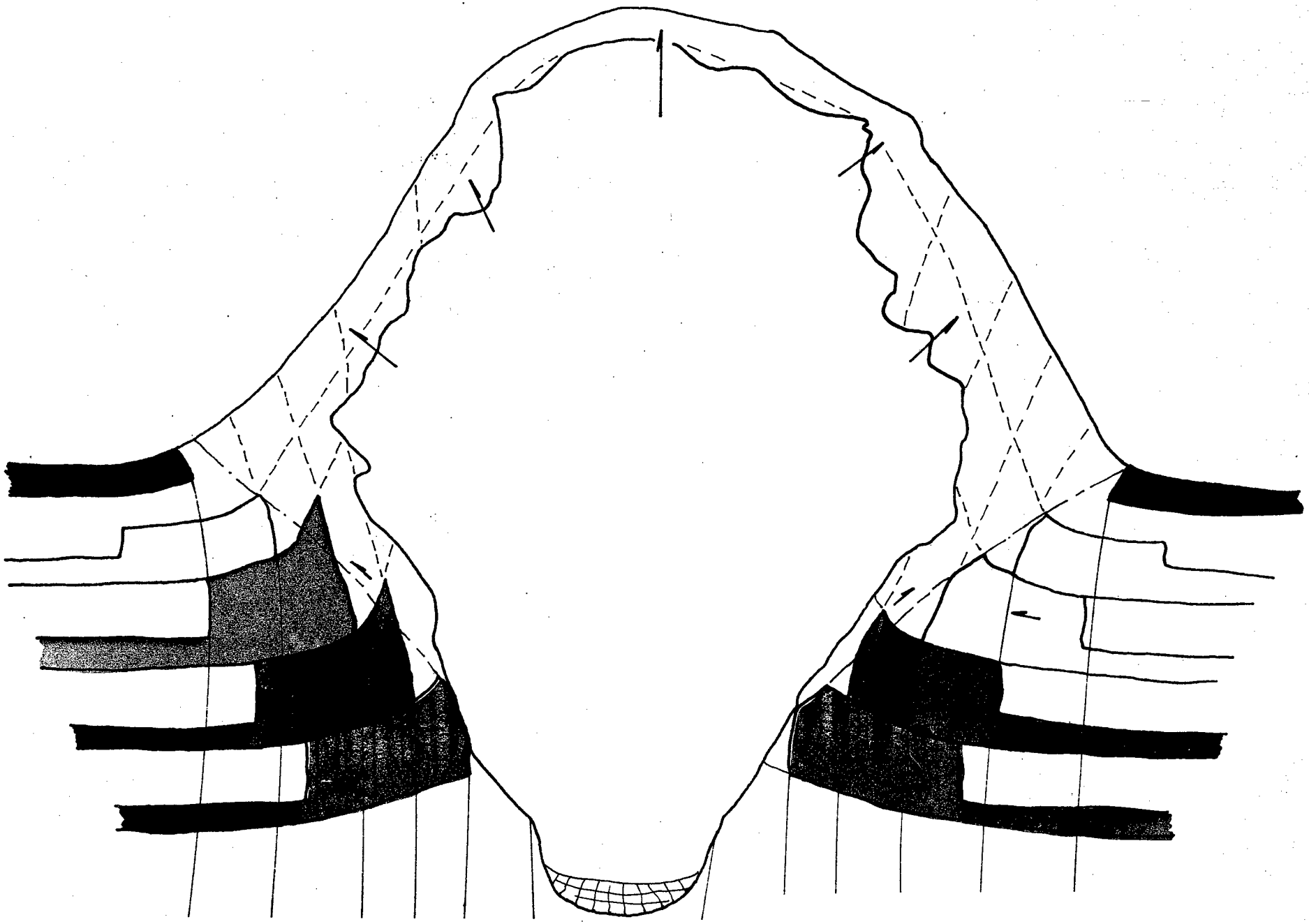

Figure 4.8 Mound growth continues at peak velocity; rebound begins at mid-depth (60 to 100 msec).

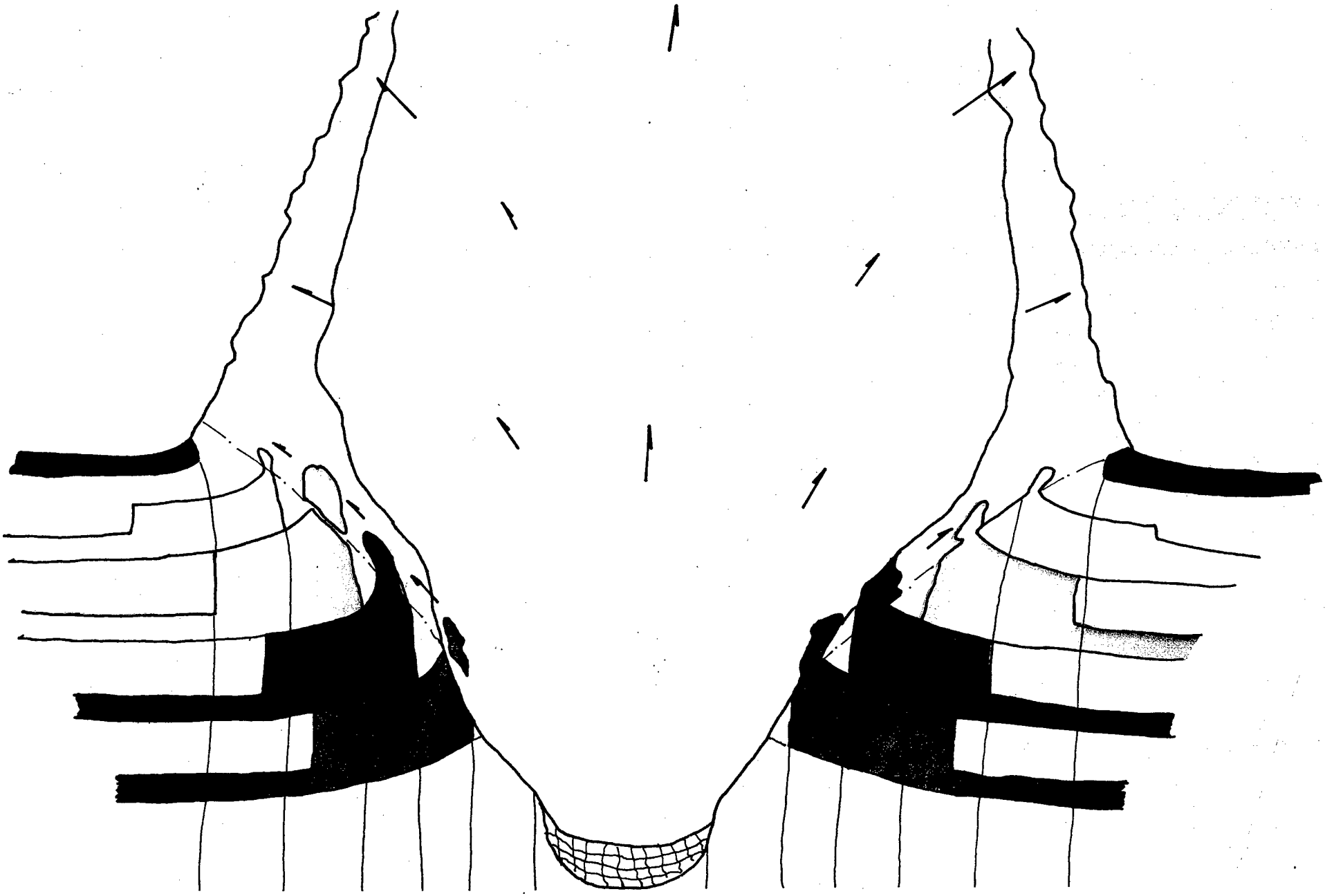

Figure 4.9 Shearing along boundary of severe deformation (125 to 175 msec).

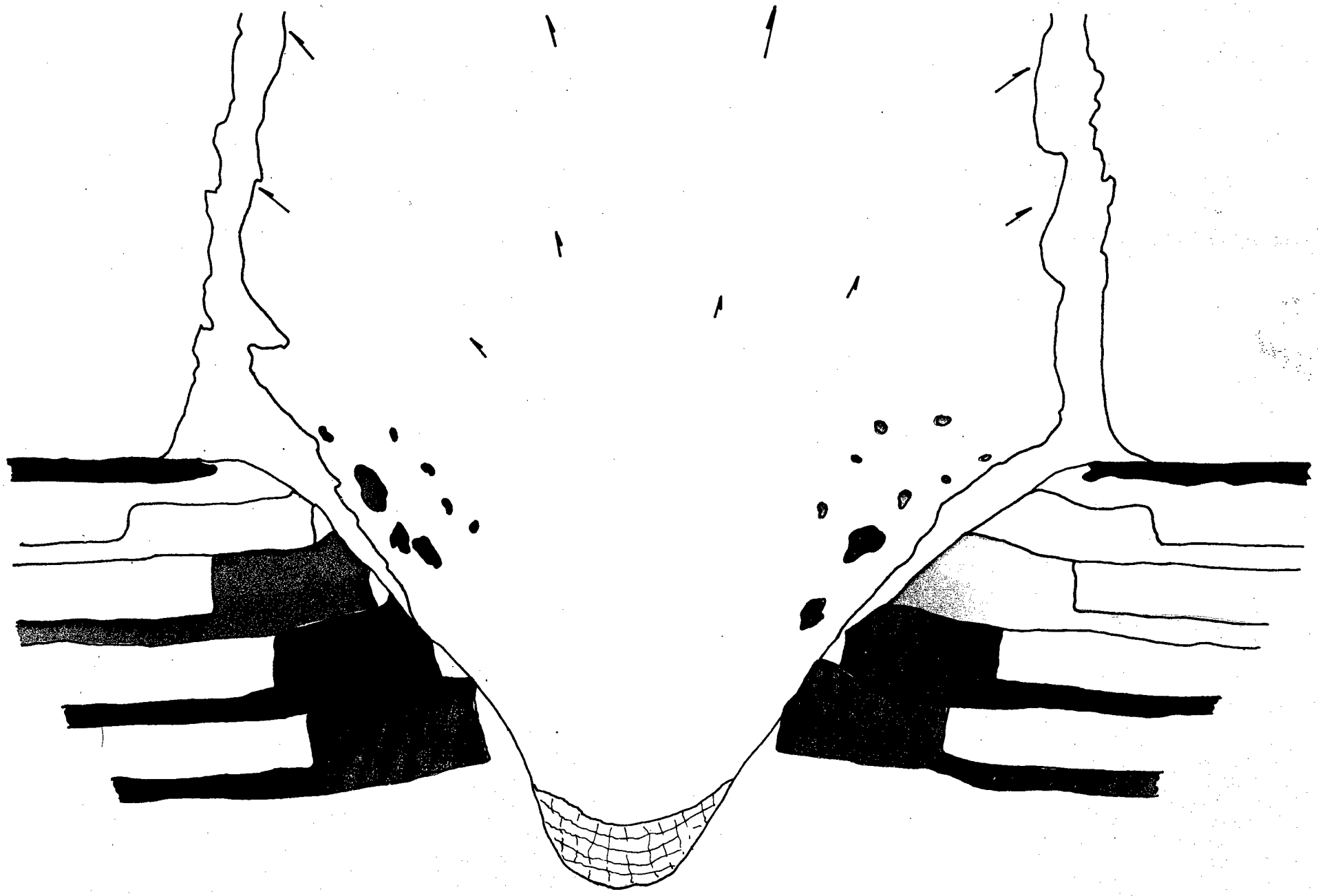

Figure 4.10 Beginning of slump along free surface slopes (250 to 300 msec).

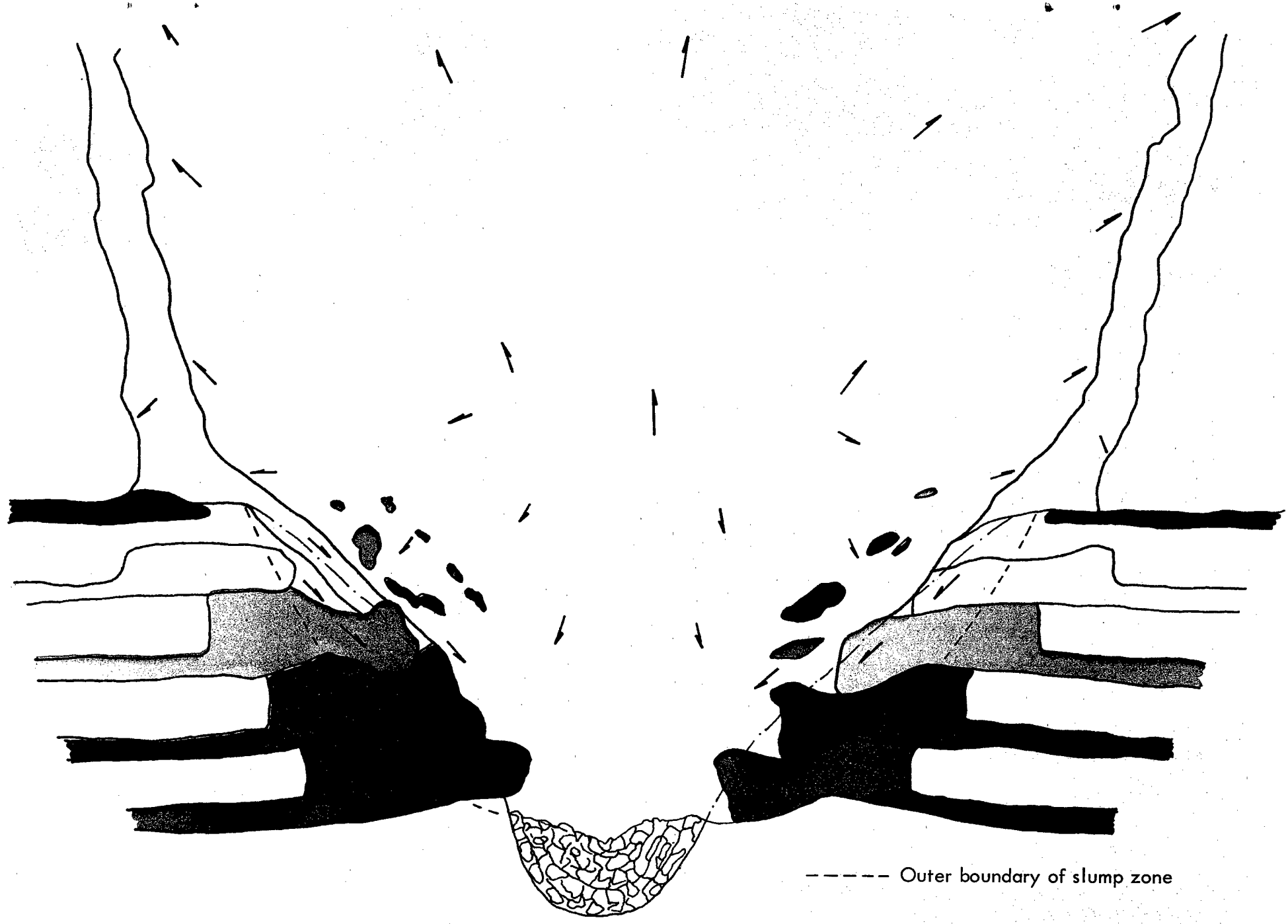

Figure 4.11 Continuing slump along free surface slopes; material fallback begins (300 to 400 msec).

expanding gases is released. The approximate outer boundary of the slump zone is shown by the dashed line. The air above the crater is filled with a large number of particles of varying size. The larger particles have begun to fall towards the bottom of the cavity.

4.2.10 End of Slump; Fallback Continues (Figure 4.12). This figure shows the final configuration of the cavity walls after the completion of the slumping process. The cavity walls have failed before the ejecta returns to the crater. The top layers have slumped below some of the highly displaced particles from deeper sand layers. The fact that large intact pieces of colored material came to rest above their preshot positions is indicative that the slumping occurred relatively early (less than 500 msec) while these particles were still in the air. After 500 msec, much of the ejecta has downward-directed velocities and the apparent crater has begun to fill with fallback material.

4.2.11 Fallback Continues to Form Crater and Lips (Figure 4.13). This figure shows the formation of the apparent crater as the fallback material settles into the cavity covering the materials which have slumped from the cavity walls. The lips of the crater are being formed by the material settling around the rim of the apparent crater.

4.2.12 Postshot Configuration (Figure 4.14). This figure shows the final crater profile as actually observed during postshot investigations in the Zulu II test pit. The apparent crater slopes are composed of the fallback materials underlain by the material which has slumped from the cavity walls. These slopes reach an equilibrium position very early in their formational history. This initial equilibrium position is then buttressed by the fallback materials.

4.3 RELATIONSHIP TO ANALYSIS OF CRATER STABILITY

The formational history of the crater and the physical characteristics and extent of the zones surrounding the crater are important to the analysis of crater stability. The description of the formation of a crater presented in paragraph 4.2 gives a qualitative insight into the physical nature of the explosion-produced crater. The crater is produced by a dynamic process which could, in fact, be described as a failure process.

The crater reaches a state of equilibrium at a very early time. This condition is further enhanced by the deposition of the fallback materials over those materials which have slumped from the cavity walls early in the formational process. As a result, it is concluded that the initial configuration of the apparent crater will be inherently stable.

To insure the satisfactory performance of a crater over the life of a project, it would also be necessary to evaluate the long-term stability. The description of the formational process presented indicates that the material surrounding the apparent crater has unique characteristics which are significantly different from those of the preshot medium. The analysis of long-term stability requires a knowledge of these postshot conditions as well as any changes which could be expected to occur in these conditions with the passage of time.

Figure 4.12 End of slump; fallback continues (400 to 500 msec).

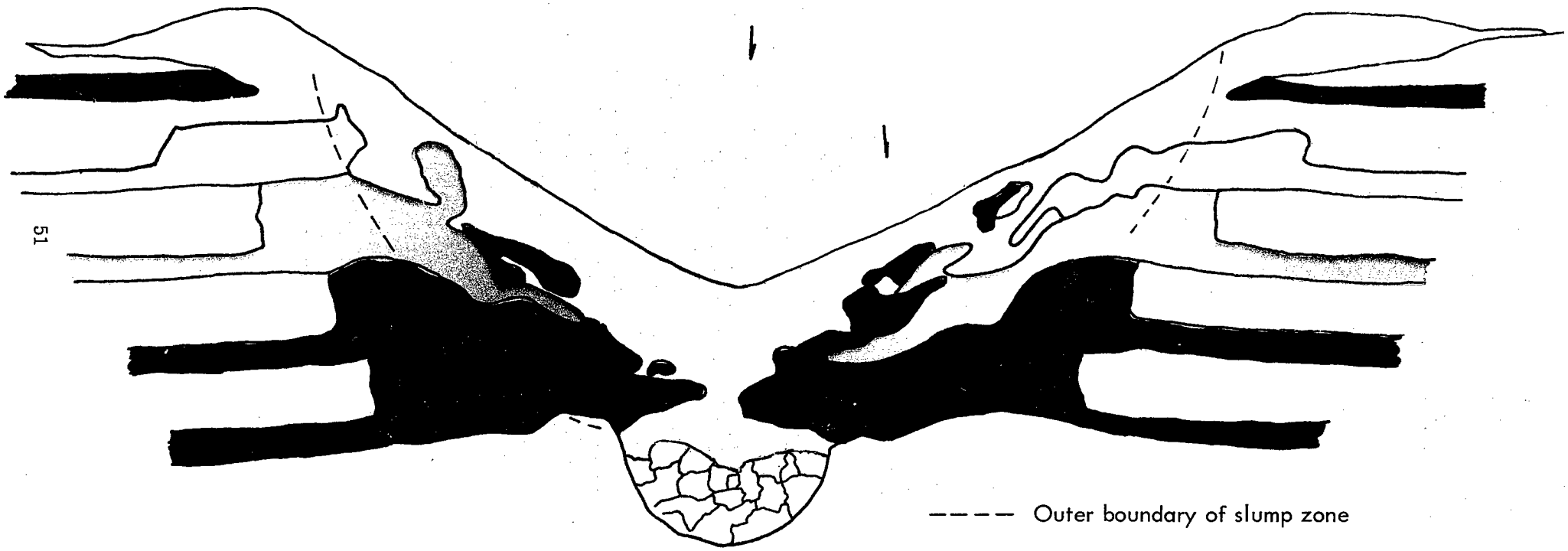

Figure 4.13 Fallback continues to form crater and lips (0.5 to 1 sec).

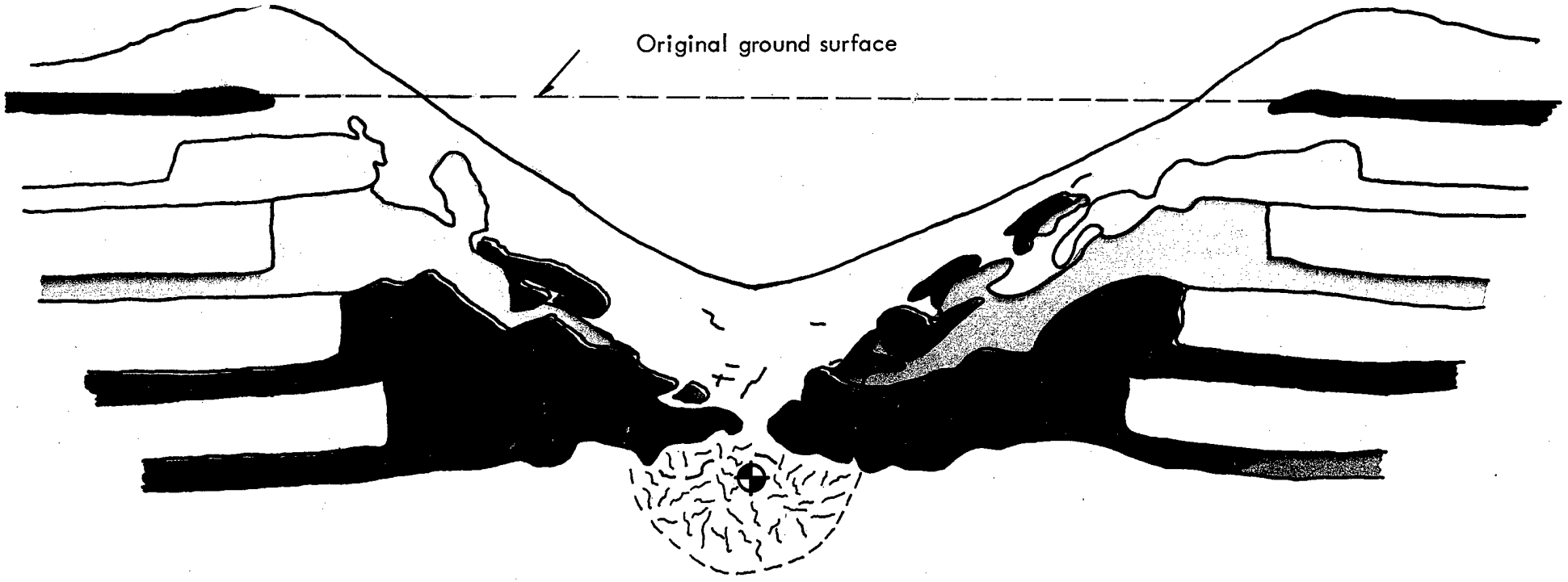

Figure 4.14 Postshot configuration.

4.4 APPLICATION TO FUTURE INVESTIGATIONS

Because of their importance to the analysis of crater stability, the mechanisms of crater formation are under continuing study. Future high-explosive experiments and their associated technical programs are being designed to test the applicability of the hypothesis of crater formation to cratering events of higher yield in different media. The results of postshot investigations of the Pre-Gondola I Bravo crater, a 20-ton high-explosive cratering event in a saturated clay shale (Reference 15) should be available in the near future. This experiment included a technical program specifically designed to test the applicability of the hypothesis of crater formation at an explosive yield level of 20 tons. The Zulu II program of laboratory-scale modeling experiments will continue to explore the phenomena of both single-charge and row-charge craters. Experience gained from these laboratory-scale experiments will be utilized in the design of larger scale cratering experiments and their associated technical programs.

CHAPTER 5
CONCLUSIONS

The laboratory-scale cratering experiments being conducted by the NCG have resulted in the development of a detailed description of the formation of an explosion-produced crater.

Half-space cratering experiments performed by Dr. Vesic of Duke University under the sponsorship of NCG have proven invaluable in the study of cratering phenomena.

Laboratory-scale cratering experiments provide a basis for the development and evaluation of the design for proposed large-scale cratering experiments and their associated technical programs.

A basis of comparison for relating the results of laboratory-scale cratering experiments to prototype nuclear excavations has been developed on the basis of geometric similarity. The ratio of D_a/DOB appears to provide an adequate basis for selecting a DOB for laboratory-scale experiments which will produce a crater with the same relative depth of disturbed material in the crater bottom as that observed in the Sedan and Danny Boy nuclear cratering events. For a one-pound charge in the Zulu II test medium, a DOB of 2.0 feet was selected. This depth is somewhat greater than the optimum DOB of 1.5 feet which produces maximum apparent crater dimensions but exposes the shot point.

The mechanism of subsidence or failure of the cavity walls has been shown to be a major factor in the formation of a crater produced by the detonation of an explosive charge buried at, or slightly below, optimum DOB.

The hypothesis of crater formation developed for a one-pound charge buried at a depth of 2.00 feet in a compact moist sand, if applicable at higher yields in different media, indicates that the initial configuration of the apparent crater will be inherently stable as a result of its formational history.

REFERENCES

1. A. B. Vesic et al.; "Theoretical Studies of Cratering Mechanisms Affecting the Stability of Crater Slopes"; Technical Report No. 3-699, October 1965; U. S. Army Engineer Waterways Experiment Station, Corps of Engineers; Vicksburg, Mississippi. (Sponsored by U. S. Army Engineer Nuclear Cratering Group.)

2. "Technical Director's Operation Plan for Project Zulu II, A Laboratory-Scale Crater Modeling Program at Site 300"; 2 August 1965; U. S. Army Engineer Nuclear Cratering Group; Livermore, California.

3. A. B. Vesic and R. D. Barksdale; "Theoretical Studies of Cratering Mechanisms Affecting the Stability of Cratered Slopes"; Final Report, Project No. A-655, 30 September 1963; Engineering Experiment Station; Georgia Institute of Technology; Atlanta, Georgia. (Prepared for U. S. Army Engineer Waterways Experiment Station, Corps of Engineers.)

4. B. C. Hughes and R H. Benfer; "Project Zulu, a One-pound High Explosive Cratering Experiment in Scalped and Remolded Desert Alluvium"; NCG/TM 65-9, October 1965; U. S. Army Engineer Nuclear Cratering Group, Livermore, California.

5. "Report of Soil Tests on Cratering Materials for Site 300"; May 1966, U. S. Army Engineer Division Laboratory, South Pacific, Corps of Engineers, Sausalito, California.

6. W. G. Christopher; "Analysis of the Phenomena Within the Immediate Crater Area Resulting from the Detonation of One-pound Zulu II Charges"; NCG/TM 66-15, April 1967; U. S. Army Engineer Nuclear Cratering Group, Livermore, California.

7. W. G. Christopher; "Analysis of Surface Motion Phenomena of One-pound Zulu II Charges at Varying Depths of Burst"; NCG/TM 66-14, 3 May 1967; U. S. Army Engineer Nuclear Cratering Group, Livermore, California.

8. M. D. Nordyke and W. Wray; "Cratering and Radioactivity Results from a Nuclear Cratering Detonation in Basalt"; UCRL-6999 Rev. II, 10 October 1963; California Univ., Livermore, Lawrence Radiation Lab.

9. M. D. Nordyke and M. M. Williamson; "The Sedan Event"; PNE 242F, 6 August 1965; Lawrence Radiation Laboratory/U. S. Army Corps of Engineers; Livermore, California.

10. M. D. Nordyke; "On Cratering. A Brief History, Analysis and Theory of Cratering"; UCRL-6578, 22 August 1961; California Univ., Livermore, Lawrence Radiation Lab.

11. "Military Engineering with Nuclear Explosives"; DASA 1669, June 1966; U. S. Army Engineer Nuclear Cratering Group; Livermore, California.

12. R. G. Bening and K. L. Larner; "Phenomenology of the Formation of a Crater by Detonation of a One-pound Charge Buried at Two Feet in Zulu II Moist Sand"; NCG/TM 66-5, February 1966; U. S. Army Engineer Nuclear Cratering Group, Livermore, California.

13. G. I. Pokrovskiy; "Explosion at Medeo, Physical Problems"; Priroda (Nature), August 1967, No. 2, 43-46. Translation, Aerospace Technology Division, Library of Congress, Washington, D. C.

14. A. N. Romashov, V. N. Rodionov, O. Yu. Shmidt; "Investigations and Results"; Priroda (Nature), August 1967 No. 2, 46-52. Translation, Aerospace Technology Division, Library of Congress, Washington, D. C.

15. M. K. Kurtz et al.; "Pre-Gondola I, Technical Director's Summary Report"; PNE 1102; U. S. Army Engineer Nuclear Cratering Group; Livermore, California; to be published.

DISTRIBUTION

LRL Internal Distribution

Michael M. May
R. Batzel
J. Bell
J. Carothers
W. Decker
S. Fernbach
J. Gofman
E. Goldberg
J. Hadley
W. Harford
C. Haussmann
R. Herbst
G. Higgins
A. Holzer
E. Hulse
J. Kane
J. Knox
J. Kury
C. McDonald
M. Nordyke 2
H. Reynolds
J. Rosengren
R. Rohrer
B. Rubin
D. Sewell
P. Stevenson
H. Tewes
J. Toman
C. Van Atta
G. Werth
D. M. Wilkes, Berkeley
E. Teller, Berkeley
TID, Berkeley
L. Crooks, Mercury, Nevada
TID File 30

External Distribution

Dr. A. S. Vesic Prof. of Civil Engineering Duke University College of Engineering Durham, North Carolina	10
D. J. Convey, Director Department of Mines and Technical Surveys Ottawa, Ontario, Canada	2
G. W. Govier Oil and Gas Conservation Board Calgary, Alberta, Canada	2
U.S. Army Engineer Division Lower Mississippi Valley Vicksburg, Mississippi	
U.S. Army Engineer District, Memphis Memphis, Tenn.	
U.S. Army Engineer District, New Orleans New Orleans, Louisiana	
U.S. Army Engineer Waterways Experiment Station Vicksburg, Mississippi	3
U.S. Army Engineer District, St. Louis St. Louis, Missouri	
U.S. Army Engineer District, Vicksburg Vicksburg, Mississippi	
U.S. Army Engineer Division, Mediterranean APO, New York	
U.S. Army Liaison Detachment New York, New York	
U.S. Army Engineer District, GULF APO, New York	
U.S. Army Engineer Division, Missouri River Omaha, Nebraska	
U.S. Army Engineer District, Kansas City Kansas City, Missouri	
U.S. Army Engineer District, Omaha Omaha, Nebraska	
U.S. Army Engineer Division, New England Waltham, Massachusetts	
U.S. Army Engineer Division, North Atlantic New York, New York	

External Distribution (Continued)

U.S. Army Engineer District, Baltimore
Baltimore, Maryland

U.S. Army Engineer District, New York
New York, New York

U.S. Army Engineer District, Norfolk
Norfolk, Virginia

U.S. Army Engineer District, Philadelphia
Philadelphia, Pennsylvania

U.S. Army Engineer Division, North Central
Chicago, Illinois

U.S. Army Engineer District, Buffalo
Buffalo, New York

U.S. Army Engineer District, Chicago
Chicago, Illinois

U.S. Army Engineer District, Detroit
Detroit, Michigan

U.S. Army Engineer District, Rock Island
Rock Island, Illinois

U.S. Army Engineer District, St. Paul
St. Paul, Minnesota

U.S. Army Engineer District, Lake Survey
Detroit, Michigan

U.S. Army Engineer Division, North Pacific
Portland, Oregon

U.S. Army Engineer District, Portland
Portland, Oregon

U.S. Army Engineer District, Alaska
Anchorage, Alaska

U.S. Army Engineer District, Seattle
Seattle, Washington

U.S. Army Engineer District, Walla Walla
Walla Walla, Washington

U.S. Army Engineer Division, Ohio River
Cincinnati, Ohio

U.S. Army Engineer District, Huntington
Huntington, West Virginia

U.S. Army Engineer District, Louisville
Louisville, Kentucky

External Distribution (Continued)

U.S. Army Engineer District, Nashville
Nashville, Tennessee

U.S. Army Engineer District, Pittsburgh
Pittsburgh, Pennsylvania

U.S. Army Engineer Division, Pacific Ocean
Honolulu, Hawaii

U.S. Army Engineer District, Far East
APO, San Francisco, California

U.S. Army Engineer District, Honolulu
Honolulu, Hawaii

U.S. Army Engineer District, Okinawa
APO, San Francisco, California

U.S. Army Engineer Division, South Atlantic
Atlanta, Georgia

U.S. Army Engineer District, Canaveral
Merritt Island, Florida

U.S. Army Engineer District, Charleston
Charleston, South Carolina

U.S. Army Engineer District, Jacksonville
Jacksonville, Florida

U.S. Army Engineer District, Mobile
Mobile, Alabama

U.S. Army Engineer District, Savannah
Savannah, Georgia

U.S. Army Engineer District, Wilmington
Wilmington, North Carolina

U.S. Army Engineer Division, South Pacific
San Francisco, California

U.S. Army Engineer District, Los Angeles
Los Angeles, California

U.S. Army Engineer District, Sacramento
Sacramento, California

U.S. Army Engineer District, San Francisco
San Francisco, California

U.S. Army Engineer Division, Southwestern
Dallas, Texas

U.S. Army Engineer District, Albuquerque
Albuquerque, New Mexico

External Distribution (Continued)

U.S. Army Engineer District, Fort Worth
Fort Worth, Texas

U.S. Army Engineer District, Galveston
Galveston, Texas

U.S. Army Engineer District, Little Rock
Little Rock, Arkansas

U.S. Army Engineer District, Tulsa
Tulsa, Oklahoma

U.S. Army Coastal Engineering Research Board
Washington, D. C.

Mississippi River Commission
Vicksburg, Mississippi

Rivers and Harbors, Boards of Engineers
Washington, D. C.

Corps of Engineers Ballistic Missile Construction Office
Norton Air Force Base, California

U.S. Army Engineer Center
Ft. Belvoir, Virginia — 10

U.S. Army Engineer Reactors Group
Ft. Belvoir, Virginia

U.S. Army Engineer Training Center
Ft. Leonard Wood, Missouri

U.S. Army Engineer School
Ft. Belvoir, Virginia

U.S. Army Engineer Nuclear Cratering Group
Livermore, California — 100

TID-4500, UC-35, Nuclear Explosions — Peaceful Applications — 292

WF:rd